journal

Developing Interfacial Phase Diagrams for Applications in Activated Sintering and Beyond: Current Status and Future Directions[‡]

Jian Luo[†]

School of Materials Science and Engineering, Center for Optical Materials Science and Engineering Technology, Clemson University, Clemson, South Carolina 29634

This article critically assesses the current status and future directions for the development of interfacial phase diagrams for applications in activated sintering and other fields. The origin of solid-state activated sintering is attributed to the enhanced mass transport in sintering-aid-based, nanoscale, quasi-liquid, interfacial films that are stabilized below the bulk solidus line. Interfacial thermodynamic models have been developed via extending a phenomenological premelting theory and incorporating the computational thermodynamic (CalPhaD) methods. A primitive type of interfacial phase diagrams, λ-diagrams, have been computed, and these diagrams have been validated by experiments and proven useful. More rigorous interfacial phase diagrams with well-defined transition lines and critical points may also be constructed. A long-range scientific goal is proposed to develop interfacial phase diagrams as a new materials science tool. Future studies should be conducted in several areas to achieve this goal, and special efforts should be made to predict the complex interfacial phase behaviors in multicomponent ceramic materials. Potential broad applications are envisaged.

I. Introduction

S INTERING aids are often used to enhance densification. If the addition of sintering aids leads to the formation of a small fraction of a liquid phase at the sintering temperature and this liquid phase wets the grain boundaries (GBs) to provide a fast mass transport pathway, the enhancement of densification can be understood by the well-established liquid-phase sintering theories.[1] However, in many systems, addition of minor sintering aids can considerably increase the densification rates when the bulk liquid phase is not yet stable.[2–7] For example, the addition of less than 1% of transition metals, such as Ni, Fe, Co, and Pd, can significantly accelerate the sintering rates of W and Mo at as low as 60%–85% of the corresponding bulk eutectic or peritectic temperatures.[2,3,5,6] Similar solid-state (subsolidus) activated sintering phenomena have also been observed in a variety of ceramic systems, including ZnO-Bi$_2$O$_3$,[7] CaF$_2$-NaF[4], and CeO$_2$-CoO[8,9] (where the primary phases are underlined). Moreover, geophysicists have long recognized the possibility of consolidation (sintering) of snow at temperatures well below the freezing point, which is often enhanced by the presence of minor impurities (although for many cases, whether the "sintering" of snow occurs above or below the bulk solidus line is not known).[10] The origin of solid-state activated sintering has been a subject of scrutiny and debate for over half a century.

In thermodynamics, melting temperatures and solidus lines are usually defined for three-dimensional bulk phases without considering the effects of finite sizes or the existence of surfaces and interfaces. Owing to the size and interface effects, transitions of nanoscale phases can often occur at conditions other than those defined by the bulk phase diagrams. As a well-known example, nanoparticles can often melt at hundreds of degrees below the corresponding bulk melting temperature.[11] When nanoscale phases are constrained, the interface effects can be even more pronounced. Thus, a nanometer-thick, sintering-aid-based, quasi-liquid, interfacial film at a GB (i.e., being sandwiched between two crystalline grains of different orientations) can be stabilized at temperatures well below the bulk solidus line under certain conditions. Enhanced mass transport rates in such GB-stabilized, sintering-aid-based, quasi-liquid, interfacial films can result in enhanced densification similar to the case of liquid-phase sintering at conditions where the bulk liquid phase is not yet stable according to the bulk phase diagram. Recent high-resolution transmission electron microscopy (HRTEM) studies directly revealed the stabilization of impurity-based, quasi-liquid, interfacial films well below the bulk solidus line in both ceramic[7,8,12,13] and metallic[5,14] activated sintering systems, which suggested that "solid-state" activated sintering is due to short-circuit diffusion in these quasi-liquid interfacial films.

In 1842, Michael Faraday already recognized the possible stabilization of a quasi-water layer on an ice surface below the freezing temperature, and he further used this phenomenon to explain the facts that two blocks of ice can freeze together and a snowball can hold together below 0°C (which are examples of "sintering"!).[10,15,16] This phenomenon of stabilization of quasi-liquid surface layers below the bulk melting temperature is known as "surface melting" or "premelting".[10,15,16] Although surface premelting had been extensively studied by physicists, materials researchers sought to confirm the existence of GB premelting. In late 1980s, Balluffi and co-workers reported[17,18] that GB premelting did not occur up to 0.999T_{melting} for pure Al. Consequently, exploration in this area was largely discouraged. In 2005, the occurrence of GB premelting in a colloidal crystal was reported.[19] GB premelting or structural disordering in unary systems has been predicted by diffuse-interface (phase-field)[20–23] and atomistic[24–29] models. Nonetheless, the existence and importance of GB premelting in real unary materials remains controversial.

Although premelting is rigorously defined for unary systems, the stabilization of impurity-based, quasi-liquid, interfacial films below the bulk solidus lines in binary and multicomponent systems is an analogous phenomenon. Furthermore, these "premelting like" films in binary and multicomponent systems can in principle be stabilized over greater undercooling or undersaturation regimes, because the structural disorder can often be promoted by concurrent solute adsorption/segregation.[12,30] Finally, the interactions between interfacial adsorption (prewetting[31]), disordering

(premelting), and layering transitions can produce complex interfacial phase behaviors.[12,32–37] Specifically, a series of discrete GB phases, namely, an intrinsic (nominally "clean") GB, a monolayer, a bilayer, a trilayer, a nanoscale intergranular film (IGF) of an equilibrium thickness, and a complete wetting film of an arbitrary thickness, have been identified by Dillon and Harmer and named as complexions[32,38–46]; the origin of this series of generic GB phases can be understood via making an analogy to a case of multilayer gas adsorption on an attractive inert substrate.[35,46,47]

Recently, interfacial thermodynamic models that combine a phenomenological premelting theory with computational thermodynamic or CalPhaD (Calculation of Phase Diagrams) methods have been developed to predict the stability of subsolidus quasi-liquid interfacial films and the related activated sintering behaviors.[48–52] Furthermore, a long-range scientific goal of developing interfacial phase diagrams, including GB and surface diagrams, has been proposed.[13,46,49,52] Such interfacial phase diagrams may have broad applications for understanding and controlling a variety of materials fabrication processing and properties.[12,13,46,49] This article critically assesses these recent developments and examines future opportunities.

This overview article first briefly discusses a phenomenological thermodynamic model that was initially developed for premelting in unary systems, where an important thermodynamic parameter, λ is defined After briefly reviewing key experimental observations of impurity-based quasi-liquid interfacial films and activated sintering, this phenomenological thermodynamic model is extended to binary and multicomponent systems to predict the stability of subsolidus quasi-liquid interfacial films and related activated sintering behaviors. Then, approaches to calculate λ-diagrams and more rigorous interfacial phase diagrams are discussed. Finally, future directions and potential applications of these interfacial phase diagrams beyond sintering are discussed.

II. Premelting in Unary Systems

The premelting phenomenon in unary systems has been extensively investigated by the physics community. The experimental observations, relevant theories, and modeling studies have been summarized in several review articles.[10,15,16,53] As illustrated in Fig. 1, quasi-liquid interfacial layers can be stabilized below the melting temperature if the free-energy penalty per unit area for forming an undercooled liquid film ($\Delta G_{amorph}^{(vol)} \cdot h$) can be over-compensated by the reduction of interfacial energies ($-\Delta\gamma$)[10,22]:

$$(-\Delta\gamma) > \Delta G_{amorph}^{(vol)} \cdot h \tag{1}$$

where h is the thickness of the quasi-liquid film. Here, the term "quasi-liquid" is used because the adjacent crystal(s) must impose some structural order to the nanoscale film; thus it is not a real liquid. For a free surface [i.e., a solid-vapor interface; Fig. 1(a)]:

$$\Delta\gamma \equiv \gamma_{lv} + \gamma_{cl} - \gamma_{cv}^{(0)} \tag{2}$$

and for a GB [Fig. 1(b)]:

$$\Delta\gamma \equiv 2 \cdot \gamma_{cl} - \gamma_{gb}^{(0)} \tag{3}$$

where γ_{cl}, γ_{lv}, γ_{cv}, and γ_{gb}, respectively, are the excess free energies for crystal-liquid, liquid-vapor, and crystal-vapor interfaces and a GB, respectively. The superscript "(0)" is used to denote a hypothetic "dry" and "perfectly crystalline"
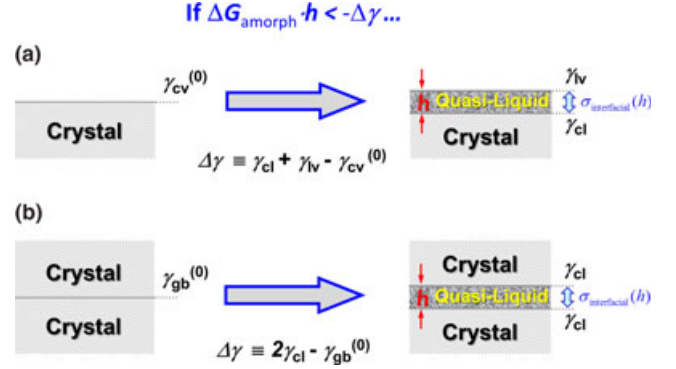

Fig. 1. Below the bulk melting temperature (or solidus line), a nanometer-thick quasi-liquid layer can be stabilized (a) on a free surface or (b) at a grain boundary if the free-energy penalty for forming the undercooled liquid film ($\Delta G_{amorph} \cdot h$) is over-compensated by the reduction in the interfacial energies ($-\Delta\gamma$).

interface, which is different from the equilibrium interface ($\gamma_{cv}^{(0)} \geq \gamma_{cv}$; $\gamma_{gb}^{(0)} \geq \gamma_{gb}$). In a phenomenological thermodynamic model,[10,22] the increase in the excess interfacial energy of a quasi-liquid interfacial film (using $\gamma_{cv}^{(0)}$ or $\gamma_{gb}^{(0)}$, and the equilibrium bulk phase(s) as the reference states) is expressed as[12,49,52]:

$$\Delta\sigma(h) = \Delta\gamma + \Delta G_{amorph}^{(vol)} \cdot h + \sigma_{interfacial}(h) \tag{4}$$

The last term in Eq. (4) is an "interfacial potential" that represents the interactions of two interfaces when the film is thin; it is the sum of all short- and long-range interfacial interactions using $h = +\infty$ as the reference point [i.e., $\sigma_{interfacial}(+\infty) \equiv 0$], but it excludes the effect of $\Delta G_{amorph}^{(vol)} \cdot h$ (which is equivalent to an attractive interaction). By definition, $\Delta\sigma(h) = 0$ so that $\sigma_{interfacial}(0) = -\Delta\gamma$. Thus, a dimensionless "interfacial coefficient" [$f(h)$] can be defined based on the following relation:

$$\begin{cases} \sigma_{interfacial}(h) \equiv (-\Delta\gamma) \cdot [1 - f(h)] \\ \Delta\sigma(h) = f(h) \cdot \Delta\gamma + \Delta G_{amorph}^{(vol)} \cdot h \end{cases} \tag{5}$$

which satisfies the boundary conditions:

$$\begin{cases} f(0) = 0 \\ f(+\infty) = 1 \end{cases} \tag{6}$$

The derivative of the interfacial potential ($d\sigma_{interfacial}(h)/dh$) is the well-known *Derjaguin disjoining pressure*. The equilibrium interfacial energy (γ_{cv} or γ_{gb}) corresponds with an equilibrium film thickness (h_{eq}) that produces the global minimum in $\Delta\sigma(h)$:

$$\begin{cases} \dfrac{d\Delta\sigma(h)}{dh}\bigg|_{h=h_{eq.}} = 0 \\ \Delta\sigma(h_{eq}) \equiv (\gamma_{cv} - \gamma_{cv}^{(0)}) \quad \text{or} \quad (\gamma_{gb} - \gamma_{gb}^{(0)}) \end{cases} \tag{7}$$

In a series of our prior studies (which were conducted for binary systems),[34,35,48–50] we proposed to define the following thermodynamic parameter:

$$\lambda \equiv -\Delta\gamma / \Delta G_{amorph}^{(vol)} \tag{8}$$

which represents the thermodynamic tendency for an interface to disorder and scales the actual (equilibrium) film thickness. For a unary system,

$$\Delta G_{amorph}^{(vol)} = \frac{\Delta H_{fusion}^{(vol)}}{T_m}(T_m - T) = \Delta S_{fusion}^{(vol)} \cdot \Delta T \qquad (9)$$

where $\Delta H_{fusion}^{(vol)}$ and $\Delta S_{fusion}^{(vol)}$ are the fusion enthalpy and fusion entropy, respectively. T_m is the melting temperature and $\Delta T \equiv (T_m - T)$ is the undercooling. Thus, λ is proportional to $(\Delta T/T_m)^{-1}$ for a unary system. If the interfacial potential/coefficient decays exponentially (for simple metals where only one short-range interaction dominates; Fig. 2(a),

$$\begin{cases} f(h) = 1 - \exp(-h/\xi_s) \\ h_{eq} = \xi_s \ln(\lambda/\xi_s) \end{cases} \qquad (10)$$

where ξ_s is a coherent length on the order of the atomic size and the premelting interfacial structure develops when $\lambda > \xi_s$. In a molecular substance (such as ice) with an un-retarded (van der Waals) London dispersion interaction, the long-range potential/coefficient falls off quadratically [Fig. 2(b)],

$$\begin{cases} f(h) = 1 - \xi_l^2/(h^2 + \xi_l^2) \\ h_{eq} \approx \xi_l(2\lambda/\xi_l)^{1/3} \end{cases} \qquad (11)$$

where ξ_l is a constant on the order of the molecular size. Note that the interfacial coefficient is Eq. (11) is often written as $f(h) = 1 - \xi_l^2/h^2$ for the limit of $\lambda \gg \xi_l$, but that expression is invalid for the limit of $h \to 0$ (where $f(h) = 1 - \xi_l^2/h^2 \to -\infty$); this singularity is a result of a continuum approximation that is used for describing the London dispersion force. In Eq. (11), an approximate phenomenological treatment is adopted to avoid this singularity and to guarantee the satisfaction of the boundary condition: $f(0) = 0$.

Figure 2 illustrates (an incomplete list of) several representative types of interfacial coefficients that will lead to different interfacial phase behaviors. In addition to two simple cases where only one (short-range or long-range) interfacial interaction dominates [Fig. 2(a) for Eq. (10) versus Fig. 2(b) for Eq. (11)], more complicated cases often exist, where the interplay of multiple interfacial interactions can produce an equilibrium thickness [Fig. 2(d)], first-order wetting [Fig. 2(e)] and prewetting [Fig. 2(f)] transitions, and layering transitions that produce a series of discrete interfacial phases [Fig. 2(c)]. Several of these cases will be discussed in detail subsequently.

Two important points should be noted to correctly understand Fig. 2. First, below the bulk solidus line, $\Delta G_{amorph}^{(vol)} \cdot h$ represents an additional (and often significant) interfacial interaction (i.e., a constant attractive pressure with the strength of $\Delta G_{amorph}^{(vol)}$) in the relative interfacial energy versus thickness curve [$\Delta\sigma(h) = \Delta\gamma \cdot f(h) + \Delta G_{amorph}^{(vol)} \cdot h$], which is not represented in Fig. 2. Second, for the cases of $\Delta\gamma < 0$ (which represent the majority of cases that are discussed herein), the minima in excess interfacial free energies often correspond to the maxima in $f(h)$ [based on Eq. (5)], which can be further shifted by the $\Delta G_{amorph}^{(vol)} \cdot h$ term.

Section IV summarizes and discusses our recent efforts in developing a primitive type of interfacial phase diagrams (what we called "λ diagrams") where the details of the interfacial coefficients are first neglected. The effects of the interfacial potentials (coefficients) are further discussed in Sections V and VI; in particular, Section VI illustrates that sophisticated models that consider the detailed interfacial interactions can produce more rigorous interfacial phase diagrams with well-defined transition lines and critical points.
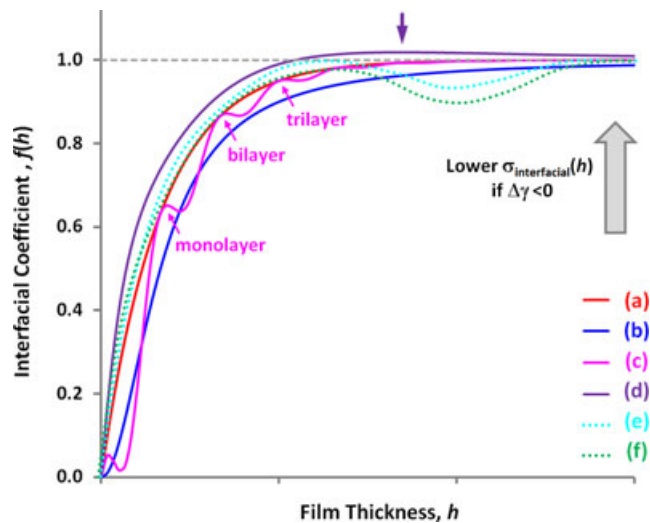

Fig. 2. Schematic illustrations of several representative interfacial coefficients (*f(h)*) for: (a) an exponentially decaying short-range interaction [Eq. (10)]; (b) a long-range interaction that represents a London dispersion force [Eq. (11)]; (c) a case where an oscillatory structural interaction leads to layering transitions and produces discrete monolayer, bilayer, trilayer *etc.* (see Section VI, Figs. 8 and 9 for further discussion); (d) a case where a repulsive short-range force and an attractive long-range force produce an "equilibrium" thickness (indicated by the purple arrow) above the solidus line; (e) a case where a first-order wetting transition occurs at the solid-liquid coexistence; and (f) a case where a first-order prewetting transition may occur below the solidus line. The dimensionless *f(h)* is related to the interfacial potential by Eq. (5). Noting that below the bulk solidus line, $\Delta G_{amorph}^{(vol)} \cdot h$ is an additional (and often significant) attractive interaction in $\Delta\sigma(h)$ that is not represented in *f(h)* and this figure.

III. Impurity-Based Quasi-Liquid Interfacial Films and Activated Sintering

Since late 1970s, ceramic and materials researchers have discovered the widespread existence of a unique class of impurity-based intergranular films or IGFs that exhibit the following distinct characteristics[12,54–57]: (1) a self-selecting or equilibrium thickness on the order of 1 nm; (2) an average film composition that differs from that of the corresponding bulk liquid/glass phase (which can sometimes lie within a bulk immiscible gap!); and (3) a quasi-liquid structure that is neither completely crystalline nor fully amorphous. These nanoscale IGFs can be alternatively interpreted as quasi-liquid interfacial films that adopt an "equilibrium thickness" in response to several attractive and repulsive interfacial forces (the Clarke model)[55–58] or disordered and discrete "multilayer adsorbates" with compositions set by bulk chemical potentials (the Cannon model).[54,58] The observations, theories, and technological importance of these nanoscale quasi-liquid interfacial films are recently reviewed.[12]

In metallic alloys, GB premelting was first indicated by the discontinuities or abnormalities in measured GB diffusivities and GB chemistry. Here, the first observation was made by studying the GB diffusion of Zn in Fe–Si bicrystals,[59] where the researchers observed a region of abnormally high diffusivities which abruptly dropped to the "normal" values at certain transition concentrations.[60–62] These abnormal diffusion behaviors were explained by assuming the existence of premelting like layers in the Fe-Si-Zn system. Consequently, several interfacial (GB) phase diagrams were experimentally constructed for the first time,[60–62] in which the GB transition lines (estimated from the diffusion data) were drawn in the bulk Fe-Si-Zn phase diagrams. Furthermore, it was demonstrated that an applied high pressure could suppress the formation of the premelting, similar to GB layers in Fe-Si-Zn[63] (and it is interesting to note that an analogous behavior of

high-pressure suppression of impurity-based IGFs was also observed in a ceramic system, ZnO-Bi$_2$O$_3$[64,65]). In addition to Fe-Si-Zn, studies have also been conducted for several other systems, particular for Cu-Bi,[33,37,66–69] where a GB phase diagram was also constructed. More recently, direct HRTEM images of impurity-based, premelting like IGFs have been obtained for several metal alloys, including W-Ni,[5,14] Mo-Ni,[50] and Nd-Fe-B.[70]

In addition to the impurity-based IGFs at GBs in ceramic and metallic materials, thin interfacial films of similar character have been directly observed by HRTEM at ceramic-ceramic,[12,71] metal-ceramic[72–76], and metal-metal[77] phase boundaries. Moreover, a class of "surficial amorphous films" (SAFs) have been discovered in a variety of oxides (as the free-surface counterparts to IGFs).[13,78–84] Similar to IGFs, these SAFs are not fully amorphous (despite being called surficial "amorphous" films) because of the significant structural order imposed by the adjacent crystalline surfaces. The observations and theories of these SAFs have been documented in a recent Annual Review article.[13] The discovery of SAFs offered a surface-GB analogy that helped to establish a unified thermodynamic framework to understand the formation mechanisms of this class of interfacial phenomena.[13]

In particular (relevance to the phenomenon of activated sintering), the stabilization of impurity-based quasi-liquid IGFs and SAFs below the bulk subsolidus lines have been observed,[5,7,14,85,86] provoking an analogy to the phenomenon of premelting in unary systems. Recently developed diffuse-interface models[12,30,87] suggested that these subsolidus IGFs and SAFs in binary systems could form from coupled interfacial premelting (disordering) and prewetting (adsorption) transitions. Electrostatic[56] and London dispersion interactions[83,88] should be separately included, resulting in more complex adsorption and wetting behaviors. Due to the presence of the attractive London dispersion forces in ceramic systems, nanoscale equilibrium thickness IGFs and SAFs can often persist above the bulk solidus line (in equilibrium with a partial-wetting bulk liquid phase)[12,13,83]; the corresponding interfacial coefficient of one such example is shown in Fig. 2(d), where a balance between an exponentially decaying short-range repulsion and a long-range attraction (London dispersion force) results in a minimum in the interfacial potential [i.e., a maximum in the interfacial coefficient, as indicated by the purple arrow in Fig. 2(d)]; thus, an equilibrium thickness is evident above the bulk solidus line (i.e., the Clarke model[55,56]). Such a unique wetting configuration has phenomenological similarities to the so-called "frustrated complete wetting",[89] "pseudo-partial wetting"[90] or "autophobic wetting"[91] phenomena. Thus, impurity-based IGFs and SAFs are not simple premelting or prewetting films. Moreover, they can also represent metastable equilibration. See recent review articles[12,13] for elaboration.

A prior study of ZnO-Bi$_2$O$_3$ provided the insight toward understanding the mysterious solid-state (subsolidus) activated sintering mechanism.[7] In this study, nanoscale quasi-liquid IGFs (and SAFs) were found to be stabilized at GBs well below bulk solidus line [Fig. 3(a)], occurring concurrently with the onset of activated sintering. This suggested that the enhanced sintering is due to the short-circuit diffusion in these subsolidus IGFs (and SAFs; noting that enhanced transport in these surficial films can facilitate the growth of sinter-necks but not densification).[7] This activated sintering mechanism has been suggested for other ceramic systems, such as CeO$_2$-CoO.[8,9] Similar IGFs and SAFs have also been observed at sinter-necks in lithium ion battery cathode material LiFePO$_4$-Li$_4$P$_2$O$_7$ (in sintered/annealed powders) [Fig. 3(b)].[84]

In the powder metallurgy community, it is commonly understood that the minor addition of certain transition metals can significantly increase the densification rates of refractory metals (such as W and Mo) in the subsolidus region,[3,4,6,92–96] and the solid-state activator was presumed to

be the secondary (bulk) crystalline phase that completely wets the GBs. Recent studies unequivocally illustrated that solid-state wetting could not occur[5,49,50]; instead, impurity-based quasi-liquid IGFs were found to be stabilized at GBs well below the bulk solidus line in W-Ni and Mo-Ni (see HRTEM images in insets in Figs. 4 and 5, and Fig. 9), which presumably led to an enhanced GB diffusion and subsolidus activated sintering.[5,48–50]

IV. Development of Interfacial λ-Diagrams for Binary Alloys

The phenomenological thermodynamic theory for premelting in unary systems described in section §II has been extended to binary systems.[48–52] In a binary alloy, one needs to select (somewhat subjectively) a reference composition [$X_{\text{film}}^{(\text{ref})}$] for a hypothetical uniform film of undercooled liquid to compute λ; the remaining excess volumetric free energies, along with the gradient energy terms, can be included in the interfacial potential to keep the thermodynamic treatment rigorous. The λ defined in Eq. (8) becomes a function of this reference film composition: for an IGF,

$$\lambda_X(X_{\text{film}}^{(\text{ref})}) \equiv \frac{\gamma_{\text{gb}}^{(0)} - 2\gamma_{\text{cl}}^{(0)}(X_{\text{film}}^{(\text{ref})})}{\Delta G_{\text{amorph}}(X_{\text{film}}^{(\text{ref})})} \tag{12}$$

and a similar λ can be defined for an SAF. The consistence of the thermodynamic model requires this reference composition to be identical to the liquidus composition (X_L) as the film thickness approaches infinity. Three possible conventions have been proposed[52]; the two commonly adopted conventions that have been used in prior studies are to select the reference film composition (1) to maximize λ[48,49] or (2) to be a constant identical to the liquidus composition (X_L)[50–52]:
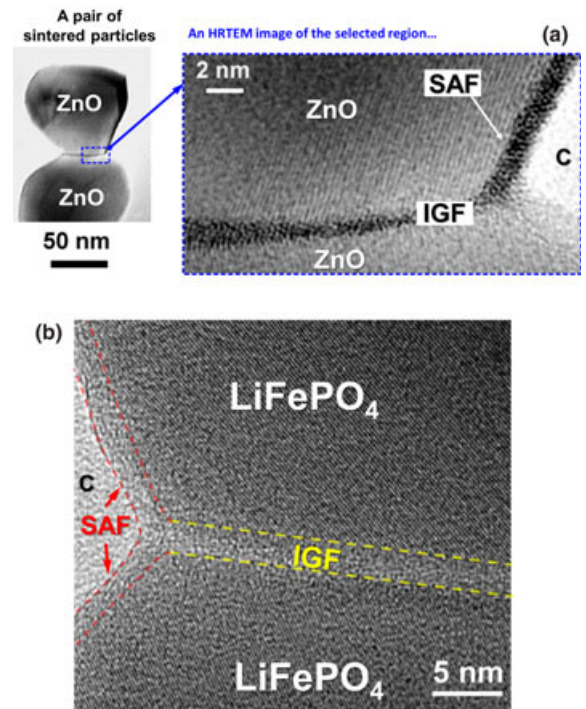

Fig. 3. (a) A pair of Bi$_2$O$_3$-doped ZnO particles that was sintered below the solidus line. A prior HRTEM study demonstrated that Bi$_2$O$_3$-based, quasi-liquid, interfacial films formed at virtually all general GBs and some surfaces.[7] (b) A HRTEM micrograph of similar Li$_4$P$_2$O$_7$-based IGFs and SAFs formed at the sinter-necks in LiFePO$_4$ based battery cathode materials.[84] Panel (b) is adapted from Ref. [84] with permission from AIP.
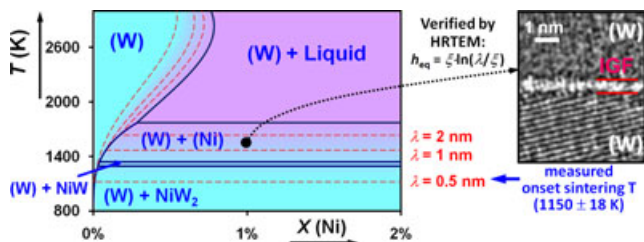
Fig. 4. A computed GB λ-diagram for Ni-doped W, in which lines of constant computed λ (the red dashed lines) are plotted in the W-Ni binary bulk phase diagram. The colors represent the thermodynamic tendency for the general GBs to disorder (i.e., the computed λ values in a continuous scale). This computed GB λ-diagram has been validated by experiments: in addition to direct HRTEM validation, the observed onset sintering temperature is coincident with the predicted GB solidus/disordering temperature (see Table I). This computed GB λ-diagram is re-plotted after Ref. [49] and the HRTEM image is adapted from Ref. [14] with permission from Elsevier.

$$\begin{cases} \lambda \equiv \underset{(0 < X_{\text{film}}^{(\text{ref})} < 1)}{\text{Max}} \left\{ \lambda_{\text{X}}(X_{\text{film}}^{(\text{ref})}) \right\} \\ \lambda_{\text{L}} \equiv \lambda_{\text{X}}(X_{\text{L}}) \end{cases} \qquad (13)$$

Both λ and λ_{L} represent the thermodynamic tendency to stabilize subsolidus quasi-liquid interfacial films. On one hand, λ appears to be conceptually more rigorous, but it needs to be quantified numerically.[48,49] On the other hand, λ_{L} is easier to quantify (with analytical expressions available

for subregular solutions).[50,52] It should be noted that the assumption of $X_{\text{film}} = X_{\text{L}}$ (for computing λ_{L}) becomes invalid for a virtually pure system; however, this problem can be circumvented with an interpolation scheme described in Ref. [52].

Computational thermodynamic (CalPhaD) methods can be used to determine the free-energy penalty for forming an undercooled liquid (ΔG_{amorph}), where the Gibbs free energy of a phase Φ in a binary A-B system can be expressed as:

$$G^{\Phi} = \sum_{i=\text{A,B}} X_i \cdot {}^{0}G_i^{\Phi} + RT \sum_{i=\text{A,B}} X_i \ln X_i + {}^{XS}G^{\Phi} \qquad (14)$$

where ${}^{0}G_i^{\Phi}$ is the Gibbs free energy of the pure element i (=A or B) that is present in Φ phase, and X_i is the atomic fraction of element i. In most cases, the subregular solution model (i.e., a Redlich-Kister polynomial where $n = 1$) can be adopted, where the excess Gibbs free energy can be as expressed as:

$$^{XS}G^{\Phi} = L_0^{\Phi} X_{\text{A}} X_{\text{B}} + L_1^{\Phi} X_{\text{A}} X_{\text{B}} (X_{\text{A}} - X_{\text{B}}) \qquad (15)$$

where L_j^{Φ}'s are parameters. If $L_0^{\Phi} = L_1^{\Phi} = 0$, the phase Φ is an ideal solution. If $L_1^{\Phi} = 0$ and $L_0^{\Phi} \neq 0$, the phase Φ is a regular solution and L_0^{Φ} (i.e., the Ω in Ref. 50) is the so-called regular solution parameter. Gibbs free-energy functions for compounds and ordered solutions can be constructed using different models. The free-energy penalty to form an undercooled liquid can be computed from the liquid formation free energy and the chemical potentials set by the
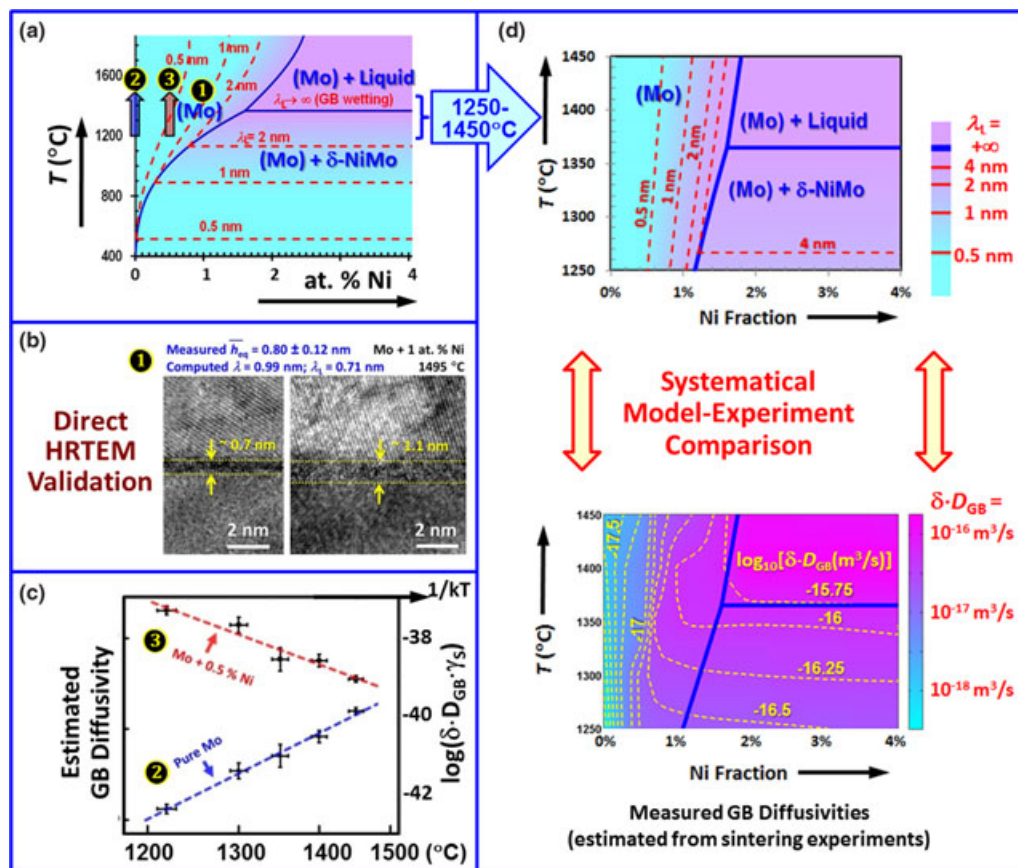

Fig. 5. (a) A computed GB λ-diagram for Ni-doped Mo, in which lines of constant computed λ_{L} [the red dashed lines; noting that $\lambda_{\text{L}} < \lambda$; see Eq. (13) for definitions] are plotted in the Mo-Ni binary bulk phase diagram.[52] (b) The existence of quasi-liquid IGFs in the single phase region has been directly verified by HRTEM [for the point labeled by ① in (a)].[50,52] (c) Furthermore, a counterintuitive prediction of decreasing GB diffusivity with increasing temperature for a Mo + 0.5 at.% Ni alloy has been confirmed by experiments (labeled by ② versus ③).[51] (d) Finally, the validity and usefulness of this computed λ-GB diagram has been confirmed by a systematical comparison with measured GB diffusivities.[52] This figure is assembled and re-plotted from the data and images reported in Refs. 51,52 with permissions from APS.

equilibrium bulk phases:

$$\Delta G_{\text{amorph.}}(X_{\text{film}}^{(\text{ref})}) = G^{\text{liquid}} - [X_{\text{film}}^{(\text{ref})}\mu_B + (1 - X_{\text{film}}^{(\text{ref})})\mu_A]$$

(16)

To compute λ, numerical calculations of both ΔG_{amorph} and $\Delta\gamma$ have to be conducted for all reference film compositions to seek for the maximum value. In an alternative approach, the reference film composition is taken to be the liquidus composition (X_L) for calculating λ_L, where a prior study derived an (almost) analytical expression for ΔG_{amorph} and λ_L for cases where the Gibbs free energy of the (primary) solid phase can be described by a regular solution model (characterized by the parameters L_0^{solid} and L_1^{solid})[52]:

$$\Delta G_{\text{amorph}}^{(\text{mol})}(X_L) = RT\left[X_L\ln\frac{X_s}{X_0} + (1 - X_L)\ln\frac{1 - X_s}{1 - X_0}\right]$$
$$- (X_S - X_0)[2X_L(L_0^{\text{solid}} + 3L_1^{\text{solid}})$$
$$- (L_1^{\text{solid}} + 3L_1^{\text{solid}} + 6L_1^{\text{solid}}\cdot X_L)(X_S + X_0)$$
$$+ 4L_1^{\text{solid}}(X_S^2 + X_SX_0 + X_0^2)]$$

(17)

where X_0 is the fraction of B in the primary phase that sets the bulk chemical potentials. X_S and X_L, respectively, are the fractions of B on the solidus and liquidus lines (or their metastable extensions), respectively. If the solid phase is a regular solution ($L_1^{\text{solid}} = 0$; $L_0^{\text{solid}} = \Omega$), Eq. (17) can be simplified to:

$$\Delta G_{\text{amorph}}^{(\text{mol})}(X_L) = RT\left[X_L\ln\frac{X_s}{X_0} + (1 - X_L)\ln\frac{1 - X_s}{1 - X_0}\right]$$
$$- \Omega(X_S - X_0)(2X_L - X_S - X_0)$$

(18)

which was derived separately in an earlier report.[50] In the above approaches, X_S and X_L have to be determined by either experiments or CalPhaD methods. In Eqs. (17) and (18), the superscript "(mol)" denotes it is a molar free energy and it relates to the volumetric free energy by:

$$\Delta G_{\text{amorph}}^{(\text{mol})} \approx \Delta G_{\text{amorph}}^{(\text{vol})}\cdot[V_B\cdot X_{\text{film}}^{(\text{ref})} + V_A\cdot(1 - X_{\text{film}}^{(\text{ref})})]$$

(19)

where V_A and V_B are the molar volumes and it is assumed (for simplicity) that the film adopts the reference composition and the mixing volume is equal to zero.

For simple systems (idealized regular solutions), the interfacial energies (γ's; $\Delta\gamma$) may be estimated by lattice-gas models.[97] Furthermore, a Miedema-type "macroscopic atom" model, which was initially developed by Benedictus, Böttger, and Mittemeijer[98,99] (as well as Liu *et al.*[100]) for studying solid-state amorphization and modified by Shi and Luo to use the equilibrium binary phases as the reference states to be more applicable to the current case,[52] has been proven to be robustly useful to estimate γ's and $\Delta\gamma$ for binary transition alloys (see Ref. 52 for the formulae and discussion). Then, λ or λ_L can be computed as a function of temperature and overall composition. Subsequently, lines of constant λ or λ_L are plotted in the bulk phase diagrams; these so-called "λ-diagrams" are a primitive type of (not rigorous) interfacial phase diagrams. Two examples of the computed GB λ-diagrams for Ni-doped W and Ni-doped Mo are shown in Figs. 4 and 5, respectively, where the computed λ or λ_L values represent the thermodynamic tendency for the average general GBs to disorder (noting that λ or λ_L is not the actual IGF thickness, but it should scale the actual film thickness).

It should be emphasized that the λ-diagrams shown in Figs. 4 and 5 represent the average behaviors of the general (low-symmetry, random) GBs. Significant GB-to-GB variations in adsorption, disordering, and phase behaviors are expected for a polycrystal, and such GB-to-GB variations can also be estimated by such a phenomenological model.[49] However, special GBs (low-angle GBs or high-symmetry special sigma boundaries) are expected to behave differently, and in general they cannot be described by the current model.

Such computed GB λ-diagrams are useful for predicting activated sintering behaviors. The correctness and usefulness of the above interfacial thermodynamic models and the computed λ-diagrams have been validated in prior studies (at least for binary refractory alloys):

1. Direct HRTEM and Auger electron spectroscopy measurements[5,14,50,52] showed that the computed λ_L and λ values provide good estimations for the average thickness of IGFs at general GBs (at least for metallic systems; see insets in Figs. 4 and 5),[5,14,48,50,52] even if λ and λ_L ($\lambda > \lambda_L$) are not h_{eq}.
2. These GB diagrams correctly predicted the onset activated sintering temperatures for a series of five W alloys (W-Pd; W-Ni; W-Co; W-Fe, and W-Cu) for which both thermodynamic data and experimental results are available in literature to enable such computation and comparison (see Table I)[48,49]; the computed λ versus temperature curves for the solid-solid two-phase region could provide furthermore detail of temperature-dependent activated sintering behaviors (see Ref. 48 for detail)
3. The predicted GB solidus temperature is coincident with a direct GB diffusivity measurement for W-Co.[48,101]
4. In a most recent study,[52] controlled sintering experiments were conducted to estimate the GB diffusivity as a function of temperature and overall composition for Ni-doped Mo, and the experimental results correlate well with the computed GB λ-diagram [Fig. 5(d)]. This provided the most systematic demonstration of the predictability and usefulness of such a λ-diagram. Most notably, a counterintuitive phenomenon of decreasing GB diffusivity with increasing temperature was predicted by this model for a Mo + 0.5 at.% Ni alloy, which was subsequently verified by experiments [Fig. 5(c)].[51]

V.   Discussion and Future Directions

Although the discussion in section §IV is mainly about computing GB λ-diagrams (in part because the densification in activated sintering is largely resulted from GB diffusion), similar models are applicable to free surfaces. Figure 6 shows an experimentally measured surface diagram for ZnO-Bi$_2$O$_3$, where lines of the constant (measured) thickness of the Bi$_2$O$_3$-enriched SAFs on the (11$\bar{2}$0) surface of ZnO are plotted in the ZnO-Bi$_2$O$_3$ bulk phase diagram. The surface diagram shown in Fig. 6 is different from the two GB

Table I.   Measured Onset Sintering Temperatures Versus Predicted GB Disordering Temperatures for Several Tungsten Based Activated Sintering Systems. Adapted from Ref. 48 with Permission of AIP

	Observed onset sintering temperature (K)	Predicted GB disordering temperature (K)
W-Pd	1090 ± 23	<1141
W-Ni	1150 ± 18	1121–1470
W-Co	1301 ± 49	1140–1644
W-Fe	1308 ± 50	1273–1664
W-Cu	No activated sintering effect	No IGF formation

λ-diagrams shown in Figs. 4 and 5 in that it represents the actual measured film thicknesses (measured h_{eq}'s; instead of computed λ or λ_L values). Nonetheless, a comparison of Fig. 6 to Figs. 4 and 5 shows analogous trends of temperature- and composition-dependence on film thickness between free surfaces and internal GBs, as well as phenomenological similarities between metallic and ceramic systems. Some differences (e.g., the divergence of film thickness at the bulk solidus line) are expected and discussed subsequently.

Although the interfacial thermodynamic models and the computed λ-diagrams discussed above have been validated by experiments and proven useful, furthermore studies should be conducted to improve these models and approaches. Several major areas of opportunities are discussed subsequently.

First, future studies should be conducted to refine, extend, and validate the interfacial thermodynamic theories for realistic modeling of ceramic systems. Although Miedema-type models are robustly useful and efficient for estimating γ's for transition metal alloys,[98–100] reliable statistical thermodynamic models for estimating γ's in oxide and non-oxide ceramic systems have yet to be developed and validated (noting that the macroscopic atom models have already been extended to estimate the surface energies of oxides[99,102]). Alternatively, γ's of ceramic systems can be obtained via experiments or first-principle calculations. Furthermore, the interfacial potentials for ceramic materials can be more complex and include multiple interfacial interactions of significant strengths:

$$\sigma_{interfacial}(h) = \sigma_{structural/chemical}(h) + \sigma_{vdW}(h) + \sigma_{elec}(h) + \sigma_{OS}(h)\ldots$$
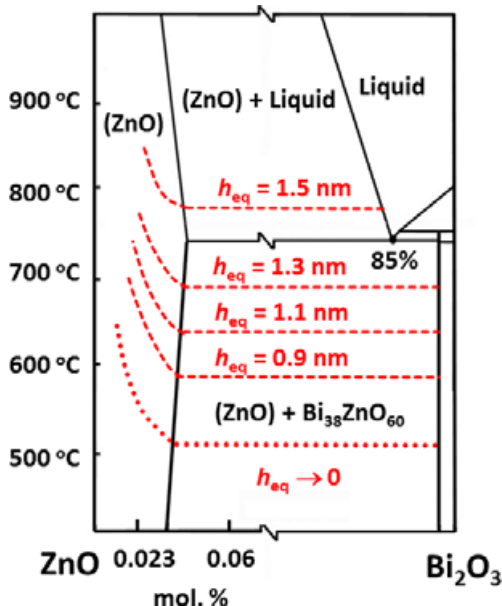
(20)

Fig. 6. A measured surface diagram for the $(11\bar{2}0)$surface of Bi_2O_3-doped ZnO, where lines of constant film thickness (red dashed lines) are plotted in the binary bulk phase diagram. Note that this diagram is different from the two GB λ-diagrams shown in Figs. 4 and 5 in that it is for SAFs (instead of IGFs), it is for a ceramic (instead of metallic) system, it is a measured (instead of computed) diagram, and it represents the actual equilibrium film thickness h_{eq} (instead of λ or λ_L). Nonetheless, some similar trends on the temperature and composition dependence of films thickness (or λ value) can be evident. The relevant data that led to the construction of this surface diagram were reported in Refs. 78–80,83,87 and this figure is re-plotted after an original diagram published in Ref. 80 with permission from ACS, in which a correction considering the newer data about the inhibition of complete wetting transition by an attractive dispersion force reported in Ref. 83 was made.

which include the relatively "short" range interactions of structural and/or chemical origins (such as the "steric" interaction derived by Clarke[55] and various refined interaction terms originated from the structural and/or chemical gradients[57,71,78,103]), a long-range van der Waals London dispersion interaction,[88] an electrostatic interaction,[56] and an oscillatory structural interaction due to the atom size effect[35]; these interfacial interactions are discussed in detail in several recent review articles.[12,13,104] It should be emphasized that these interfacial interactions are written as independent terms in Eq. (20) for simplicity, although they are in fact often coupled. In ceramic systems, the interfacial interactions can give rise to complex interfacial phase behaviors. For example, Fig. 6 shows that the nanoscale SAFs persist into the solid-liquid two-phase region, where the film thickness is limited by an attractive dispersion force of significant strength.[83] In this regard, perhaps the detailed shape in the interfacial potential/coefficient has to be considered in addition to the computed λ value to predict the exact interfacial behaviors for ceramic systems [e.g., the interfacial coefficient shown in Fig. 2(d) can be used to explain the persistence of nanoscale equilibrium thickness SAFs above the solidus line as shown in Fig. 6], whereas the computed λ value alone appears to be a better estimator of the effective interfacial width for simpler metallic systems (e.g., Figs. 4 and 5).

Second, future studies should be conducted to extend current approach to compute λ-diagrams for multicomponent systems (with three or more components). This is of great practical importance because engineering materials often have multiple components and impurities. Furthermore, understanding the interactions of two or more adsorbates at the interfaces and how they affect the interfacial phase behaviors can help to develop co-doping strategies to adjust interfacial structures to achieve desirable properties. Specifically, we should generalize the statistical thermodynamic models (or use first-principle or experimental methods) to obtain γ's for multicomponent systems. Then, we can integrate multicomponent CalPhaD methods to compute the free-energy penalty for forming an undercooled liquid for an N-component system:

$$\Delta G_{amorph} = G^{liquid} - \sum_{i=1}^{N} X_{film,i}^{(ref)} \mu_i$$

(21)

where $X_{film,i}^{(ref)}$ and μ_i are the reference film composition and the bulk chemical potential of the ith component. Here, the Redlich–Kister–Muggianu procedure[105] can be used to extrapolate the formation free energy. For example, the formation free energy of a phase Φ in a ternary A-B-C system can be written as[105]:

$$G^{\Phi}(T, X_A, X_B) = X_A G_A^0 + X_B G_B^0 + X_C G_C^0 + RT(X_A \ln X_A$$
$$+ X_B \ln X_B + X_C \ln X_C) + X_A X_B \sum_{j=0}^{n_{AB}} L_j^{AB}$$
$$(X_A - X_B)^j + X_B X_C \sum_{j=0}^{n_{BC}} L_j^{BC}(X_B - X_C)^j$$
$$+ X_C X_A \sum_{j=0}^{n_{CA}} L_j^{CA}(X_C - X_A)^j + X_A X_B X_C G^{ABC}$$

(22)

where L's are binary interaction parameters and G^{ABC} represents a three-body interaction (that is typically small). Equation (22) can be readily generalized for $N > 3$. Other terms, such as the magnetization energy, can also be incorporated as needed. We can then use the well-established bulk CalPhaD methods[105] to compute the bulk chemical potentials μ_i and

ΔG_{amorph} via Eq. (21) and then the λ or λ_L values to construct λ-diagrams for multicomponent systems.

Third, studies should also be conducted to develop models and approaches to calculate more rigorous and realistic interfacial phase diagrams with well-defined transition lines and critical points (in addition to the λ-diagrams discussed above, which only represent the thermodynamic tendency for interfacial disordering); this will be discussed in the following section (VI).

Finally, it should be noted that most of the prior studies (as well as those efforts discussed in the next section, VI) have been focused on systems where the impurities or alloying elements have limited solubilities in the primary solid phases; thus they intend to form "discrete" interfacial phases. Interfacial behaviors of systems with significant solubilities in the solid phases (so significant segregation/adsorption can be accommodated within the lattice structure of the bulk crystalline phases) should be investigated separately with scrutiny.

VI. Development of More Rigorous Interfacial Phase Diagrams: First-Order Interfacial Transitions and Discrete Interfacial Phases

Although computed λ-diagrams (such as those shown in Figs. 4 and 5) are robustly useful, they are not rigorous interfacial phase diagrams with well-defined phase boundaries. As noted earlier, the computed values of λ and λ_L represent thermodynamic tendency to stabilize quasi-liquid interfacial films, and the computations of λ and λ_L do not consider the details in the interfacial potential/coefficient (therefore details of interfacial interactions are not represented). The differences between λ (or λ_L) and h_{eq} can be greater for ceramic systems; for example, as λ or λ_L approaches infinity, h_{eq} can still be at ~1 nm if there is an attractive long-range dispersion interaction of significant strength (which is not considered in calculating λ or λ_L) that prevents the occurrence of complete wetting (see Fig. 6 for an example),[12,13,83] which can be explained from an interfacial coefficient shown in Fig. 2(d). Because the interfacial forces are not considered in computing λ-diagrams; first-order transitions, the existence of which have been suggested by diffuse-interface models[20,30,34,87] and experiments,[33,37,67,81,82,106,107] cannot be described by the computed λ-diagrams. Moreover, through-thickness compositional and structural gradients generally exist in these nanometer-thick interfacial films, which are not considered in the sharp-interface approaches (except that they can be included in the interfacial coefficient partially).

In 1977, Cahn[31] developed a critical point wetting model using a diffuse-interface approach. By means of analyzing a binary de-mixed liquid system [Fig. 7(a)], Cahn elegantly demonstrated that a first-order wetting transition exists in the two-phase region, and this wetting transition line [the blue dashed line in Fig. 7(a)] extends into the single-phase phase region as a prewetting line [the blue dotted line in Fig. 7(a)]. The prewetting line corresponds to a finite (abrupt) jump in the surface adsorption amount, as shown in Fig. 7(b); thus, it is a first-order interfacial phase transition. Furthermore, this first-order prewetting line ends at a surface critical point, where this finite jump in the surface excess vanishes (beyond which the interfacial transition becomes
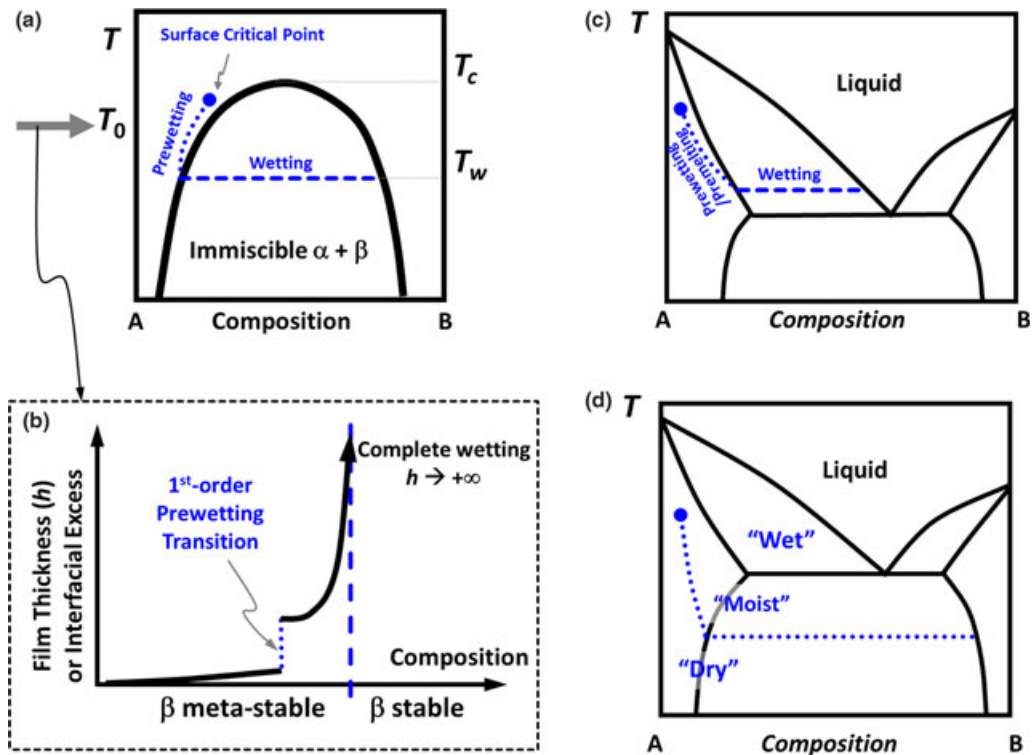

Fig. 7. Several interfacial phase diagrams predicted by diffuse-interface models. (a) Schematic illustration of the key predictions of Cahn's critical point wetting model for surface adsorption in a binary liquid system with a miscibility gap.[31] (b) An isothermal cross section at T_0 of panel (a), where the prewetting transition responds to an abrupt jump in the surface excess (i.e., the effective thickness of the adsorption film). (c) and (d) are schematic illustrations of GB phase diagrams that are similar to those constructed by Tang *et al.*[30] and Mishin *et al.*[34] for binary alloys with eutectic reactions; they predicted the existence of a coupled prewetting (adsorption) and premelting (structural disordering) transition lines. The diagram shown in (c) can be considered as a direct analogy to (a), whereas a derivative case where the wetting transition occurs below the bulk eutectic temperature is shown in (d). In (d), three distinct regions of interfacial phenomena – "dry", "moist", and "wet"—may occur in a sequence, as originally proposed by Cannon,[54] although in real ceramic systems, the complete wetting can often be delayed or inhibited by the presence of long-range attractive dispersion forces, which are not included in diffuse-interface models. In addition to the GB phase diagrams, analogous surface diagrams have also been constructed.[87] The relation between prewetting/premelting transitions predicted by diffuse-interface models and experimentally observed impurity-based IGFs and SAFs is discussed in two recent reviews.[12,13]

continuous). The corresponding (schematic) interfacial coefficients for the cases of first-order wetting and prewetting transitions are shown in Figs. 2(e) and (f), respectively; in both cases, the first-order transitions originate from the multiple minima in excess interfacial free energy versus thickness curves [i.e., maxima in the $f(h)$ in cases of negative $\Delta\gamma$, as shown in Figs. 2(e) and (f)]. These examples also illustrate that the diffuse-interface effects can be partially considered in the $f(h)$ term in a sharp-interface model, if approximate expressions for the interfacial coefficient $f(h)$ [or interfacial potential $\sigma_{\text{interfacial}}(h)$] that capture the key underlying physics can be developed.

Following Cahn's model [Figs. 7(a) and (b)],[31] two elegant diffuse-interface models have recently been developed for binary alloys by Tang *et al.*[30] and Mishin *et al.*,[34] where rigorous GB phase diagrams have been constructed; two possible examples are schematically shown in Figs. 7(c) and (d). These models revealed the existence of coupled GB prewetting and premelting transitions, which are first-order interfacial transitions with abrupt jumps in the interfacial adsorption amount (interfacial excess of solute), effective interfacial width, and structural disorder at the GB core. Similar surface diagrams have also been constructed using a diffuse-interface model,[87] which again demonstrated the surface-GB analogy. Cannon[54] further proposed that three distinct regions of interfacial phenomena—"dry", "moist", and "wet"—can occur in a sequence. This is exemplified in Fig. 7(d) (as an idealized example). The experimentally observed impurity-based IGFs and SAFs might correspond to the "moist" region in Cannon's terminology.[54] However, in real systems (particularly ceramic GBs), complete wetting can often be delayed or inhibited by the presence of long-range attractive dispersion forces, which are not included in diffuse-interface models; thus, Fig. 7(d) should be modified substantially and nanoscale IGFs and SAFs of an "equilibrium" thickness can often persist above the solidus line [for which a possible interfacial coefficient is illustrated in Fig. 2(d)]. See two recent reviews[12,13] for further elaboration.

Experimentally, evidence for the existence of a first-order surface interfacial transition from "dry" surfaces for nanoscale SAFs ("moist" surface) has been obtained for V_2O_5 on TiO_2,[81,82] which exhibits character that is consistent with the predicted coupled prewetting and premelting transitions. Most recently, evidence for the existence of a first-order interfacial transition from a nominally "clean" GB to a bilayer has been obtained for Si-Au,[107] which is somewhat different from that predicted from diffuse-interface models.

More recently, a model that considered (1) the through-thickness gradients, (2) a simplified atomic size effect (assuming that atoms are hard spheres), and (3) additional interfacial interactions (such as dispersion and electrostatic interactions) was developed for computing GB phase diagrams with discrete interfacial phases.[35] Following a diffuse-interface approach,[30,108] this model considered three field variables: composition (X), crystallinity (η), and orientation (θ). The atomic layers inside the grains are assumed to be discrete, but the liquid-like IGF exhibit continuous $X(x)$ and $\eta(x)$ profiles. At a fixed temperature (T) and bulk composition (X_B), the equilibrium GB structure is obtained by minimizing the excess free energy[35]:

$$\gamma_{\text{GB}}(T, X_B) = \min_{(\eta_i, X_i, h_0)} \left\{ 2\delta \sum_{i=2}^{\infty} \left[\Delta f_V(X_i, \eta_i) + \frac{\kappa_X}{\delta^2} \cdot (X_i - X_{i-1})^2 \right. \right.$$
$$\left. + \frac{\kappa_\eta}{\delta^2} \cdot (\eta_i - \eta_{i-1})^2 \right] + \sigma_{\text{CORE}}(X_1, \eta_1, h_0)$$
$$+ \sigma_{\text{INT}}(h) \right\}$$

(23)

where Δf_V is the excess volumetric free energy, and κ_X and κ_η are coefficients for gradient energy coefficients. The excess

free energy of a liquid-like GB core is written in a diffuse-interface model following Tang, Cannon, and Carter[30,35]:

$$\sigma_{\text{CORE}}(X_1, \eta_1, h_0) \equiv \delta \cdot \Delta f_V(X_1, \eta_1)$$
$$+ \min_{\eta(x), X(x)} \left\{ 2 \int_0^{h_0/2} \left[\Delta f_V(X(x), \eta(x)) \right. \right.$$
$$\left. \left. + \kappa_X \cdot \left(\frac{dX}{dx}\right)^2 + \kappa_\eta \cdot \left(\frac{d\eta}{dx}\right)^2 \right] dx + s\Delta\theta \cdot \eta_0^2 \right\}$$

(24)

The $X(x)$ and $\eta(x)$ profiles that minimize $\sigma_{\text{CORE}}(X_1, \eta_1, h_0)$ can be obtained by solving the corresponding Euler equations. Additional interfacial interactions [$\sigma_{\text{INT}}(h)$, which represent all interactions in the interfacial potential in Eq. (20) except for the term that arises from the structural and chemical gradients] include a term representing an atomic size effect and, for ceramics, dispersion and electrostatic interactions.[35] This model produced a systematical spectrum of GB transitions and critical phenomena [Figs. 8(a) and (b)].[35] Furthermore, it produced a series of discrete GB phases, namely: intrinsic GBs, monolayers, bilayers, trilayers, nanoscale IGFs, and complete wetting films[35]; this series of GB phases was observed in doped Al_2O_3 by Dillon and Harmer and named as complexions.[32,38–41,46] The origin of this series of discrete GB phases can be understood via an analogy to a case of multilayer surface adsorption on an attractive, inert substrate[47] (Fig. 8).

Figure 9 further illustrates the physical origin of these discrete Dillon-Harmer complexion types. First, three of the six Dillon-Harmer complexion types: intrinsic (nominally "clean") GB, monolayer adsorption, and complete wetting, are well known. Second, the existence of nanoscale equilibrium-thickness IGFs is also widely accepted now. Third, the bilayers and trilayers can be considered derivatives of IGFs with discrete thickness, if layering transitions occur (Figs. 8 and 9). Finally, if the proposed surface-GB analogy (Fig. 8) is indeed valid, this series of discrete GB phases should exist in simpler metallic alloys; recent studies have confirmed this (Fig. 9).[109]

It should be further noted that with the decreasing (effective) interfacial width, the interfacial phase would likely become more ordered (e.g., the bilayer and trilayer in Fig. 9) and less "liquid-like." It should be reiterated that even nanoscale IGFs and SAFs exhibit significant structural order (imposed by the adjacent crystals) and their structures should not be considered as full amorphous/glass or true liquid.

The above model and physical concepts for understanding the origin of discrete GB phases (Figs. 8 and 9) are still not sufficiently realistic because they adopted a colloidal-type interaction derived for hard spheres as the oscillatory structural interaction that produced layering transitions. Although such an interaction is perhaps a reasonable approximation for noble gas molecules adsorbed on an inert surface [Figs. 8(c) and (d)], adsorbates at GBs cannot be approximated as hard spheres as they form bonds with neighboring atoms. Consequently, real materials systems may not exhibit the simple and regular behavior as shown in Figs. 8(a) and (b), and 9. Consistently, a recent study observed a first-order interfacial transition from an intrinsic GB to a bilayer in Si-Au in absence of the intermediate state of a monolayer, the origin of which can be explained from the relative bond strengths based on a lattice-gas model.[107] More realistic models may be further developed along this line.

Yet another important type of important interfacial phase transition (that has not yet been considered by the present model) is the roughening/faceting transition (note the "roughening" here is different from the "roughening" in multilayer adsorption shown in Fig. 8). It is well known that surfaces can undergo roughening and faceting transitions.[110] GB roughening transitions were analyzed by Cahn[111] and more

recently by Daruka and Hamilton.[112] Kang *et al.*[113–123] have conducted systematic investigations on the roles of roughening/faceting transitions on grain growth and microstructural development.

Finally, whereas more sophisticated models and rigorous interfacial phase diagrams can provide important physical insights regarding the interfacial phase behaviors, in this author's personal opinion, the simplified λ-diagrams
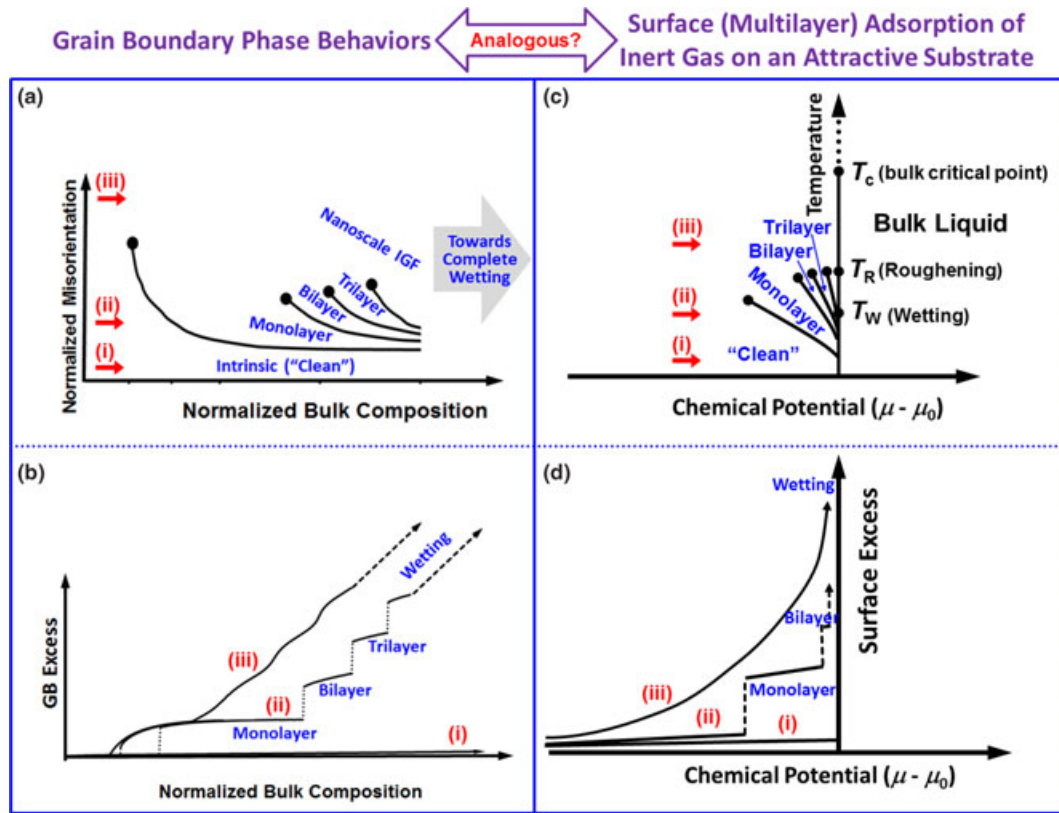

Fig. 8. (a) A computed GB phase diagram and (b) the corresponding GB excess versus normalized bulk composition (which represents the chemical potential) curves for three selected GBs labeled in (a). The GB phase behaviors shown in (a) and (b) are analogous to a case of multilayer surface adsorption of noble gas molecules on an attractive inert substrate (as illustrated by a lattice-gas model in Ref. 47 for an "intermediate-substrate" system): (c) a schematic surface phase diagram and (d) the corresponding (schematic) surface excess versus chemical potential curves for three selected temperatures labeled in (c). Panels (a) and (b) are re-plotted after Ref. 35 with permission from the AIP and panels (c) and (d) are re-reprinted from Ref. 47 with permission from APS.
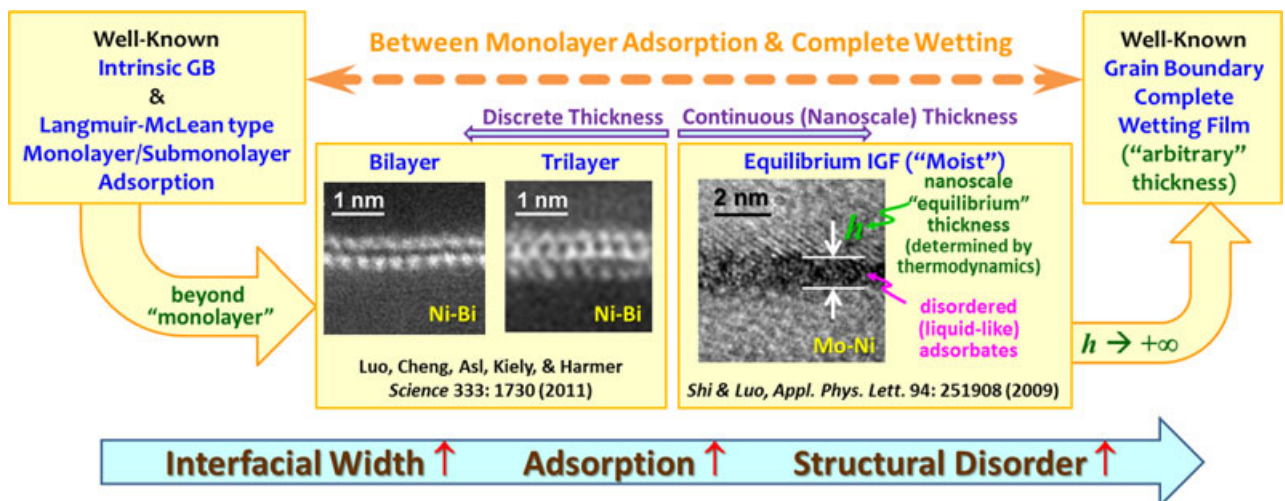

Fig. 9. Schematic illustration of the thermodynamic origin and character of a series of GB phases. Three type of GB interfacial phases, intrinsic (nominally "clean"), Langmuir-McLean (or other derivative types of) "monolayer" adsorption, and complete wetting films, are well known. If a liquid phase completely wets GBs above the solidus line, liquidlike nanoscale films can be thermodynamically stabilized at GBs below the solidus line (or such nanoscale equilibrium IGFs can persist above the bulk solidus line if their thickness is limited by an attractive long-range London dispersion, as originally proposed by Clarke[55]). Via surface analogs, one may further expect stepwise adsorption in certain systems, producing additional discrete interfacial phases, such as bilayers and trilayers. This series of generic GB interfacial phases were first observed in doped Al_2O_3 by Dillon and Harmer and named as "complexions."[32,38,39] More recently, all of them have been observed in simpler metallic systems, where the interpretation of their physical origins and microscopic images are less equivocal. Micrographs are adapted from Ref. 50 with permission from the AIP and Ref. 109 with permission from AAAS.

(although they are not rigorous interfacial phase diagrams) may remain an effective and efficient tool for predicting useful trends to guide many practical applications.

VII. Concluding Remarks and Potential Applications Beyond Sintering

The origin of solid-state activated sintering is attributed to the enhanced mass transport in sintering-aid-based, nanoscale, quasi-liquid, interfacial films that are stabilized at GBs (and surfaces) below the bulk solidus line. Since 2008, a series of studies have developed interfacial thermodynamic models and approaches to compute λ-diagrams to predict the stability of subsolidus quasi-liquid interfacial films and related solid-state activated sintering behaviors. More sophisticated models may also be developed to construct more rigorous interfacial phase diagrams with well-defined phase boundaries to describe the stability of discrete interfacial phases (complexions). The necessity of developing such interfacial phase diagrams is demonstrated by studies of activated sintering of ceramics[7] and metals[5]: since nanoscale quasi-liquid IGFs can form well below the bulk solidus lines and result in enhanced sintering behaviors similar to liquid-phase sintering,[48] bulk phase diagrams are not adequate for designing activated sintering protocols. On the other hand, recent studies demonstrated that the onset activated sintering can indeed be predicted from the computed GB λ-diagrams (see Table I and Fig. 4 for examples).[48–52]

These λ-diagrams and more rigorous interfacial phase diagrams can be a new tool for mechanism-informed materials design, with potentially broad applications beyond sintering. First, interfacial phase diagrams (including λ-diagrams) can provide information for forecasting GB-based high temperature materials properties, such as creep, oxidation, and corrosion resistance.

Second, understanding the interfacial phase behaviors may help to comprehend microstructure or morphology development; thus, interfacial phase diagrams may provide information for designing fabrication protocols to utilize the most appropriate interfacial structures to achieve optimal microstructures and/or morphologies. This is because interfacial phase formation and transition can often radically alter the kinetic process and interfacial transport rates. For example, GB adsorption can induce an interfacial structural transition to form a more disordered interfacial structure with higher transport rates, thereby promoting GB migration. This mechanism, which differs from the classical solute-drag model, has been observed for doped Al_2O_3[32,40,86] and Al-Ga.[124,125] Moreover, the existence of two or more GB complexions (as a result of GB-to-GB variation and/or metastability) with significantly different GB mobilities can lead to detrimental abnormal grain growth.[32,40,41,44,45] As another example, the formation of nanoscale SAFs can help to control the morphology of nano-particles.[13,78,79,126]

Third, interfacial phase diagrams can help to intentionally design co-doping strategies and/or heat-treatment protocols to adjust interfacial structures to achieve the desired properties. This is based on the fact that (1) interfacial phase formation and transition can often significantly alter mechanical and physical properties and (2) impurity-based interfacial phases can be retained upon cooling. It is now well known that the control of IGFs is critical for achieving room-temperature toughness and yet optimizing high temperature creep resistance for Si_3N_4 based ceramics.[127–129] For SiC-based ceramics, drying/crystallizing IGFs leads to increased creep resistance at the expense of fracture toughness.[130] IGFs and other types of GB phases (such as monolayers, bilayers, and trilayers) can play critical roles in the erosive wear resistance of Al_2O_3,[131,132] the superplasticity of Y_2O_3-stabilized ZrO_2,[133] and embrittlement of metals such as W-Ni, Mo-Ni, Cu-Bi, and Ni-Bi[5,14,33,37,50,109] as well as WC-Co cermet composites.[134] In functional materials, impurity-based IGFs and presumably other GB phases (complexions) can critically affect the tunable conductivities for ruthenate based thick-film resistors,[135] non-linear I-V characteristics for ZnO-Bi_2O_3-based varistors,[65,85] thermal conductivity of AlN substrates,[136,137] and critical currents of high T_c superconductors.[138] In general, understanding the stability of these interfacial phases and development of interfacial phase diagrams can help to control the mechanical and physical properties of the above-mentioned (and many other) conventional materials as well as develop new classes of "interfacial materials" to achieve superior properties that are not attainable by bulk phases. To support the latter claim, recent studies showed that IGFs can be utilized to increase the proton conductivity of solid-state electrolytes[139] and the magnetic properties of Nd-Fe-B[70] and SAFs can be utilized to improve the rate capabilities of lithium ion battery cathode materials,[84,140–142] and the photocatalytic properties of TiO_2 nanoparticles[143]; in all four instances, superior properties unattainable by conventional bulk phases have been achieved.

To achieve the above goals, systematic studies have to be conducted to develop and validate more realistic and predictive interfacial thermodynamic models and develop interfacial phase diagrams, particularly for complex multicomponent ceramic systems. In this author's opinion, the λ-diagrams, although not rigorous interfacial phase diagrams with well-defined transitions lines, will remain a highly valuable tool for robustly predicting some useful trends.

References

[1]R. M. German, *Liquid Phase Sintering*. Plenum Press, New York, 1985.

[2]H. W. Hayden and J. H. Brophy, "Activated Sintering of Tungsten with Group VIII Elements," *J. Electrochem. Soc.*, **110**, 805–10 (1963).

[3]R. M. German and Z. A. Munir, "Enhanced Low-Temperature Sintering of Tungsten," *Metall. Trans.*, **7A** [12] 1873–7 (1976).

[4]R. L. Coble and R. M. Cannon, "Current Paradigms in Powder Processing," pp. 151–70. in *Processing of Crystalline Ceramics*, Edited by H. Palmour III, R. F. Davis, and T. M. Hare. Plenum P., NY, 1978.

[5]V. K. Gupta, D. H. Yoon, H. M. Meyer III, and J. Luo, "Thin Intergranular Films and Solid-State Activated Sintering in Nickel-Doped Tungsten," *Acta Mater.*, **55**, 3131–42 (2007).

[6]R. M. German, "Activated Sintering of Refractory Metals by Transition Metal Additions," *Rev. Powder Metall. Phys Ceram.*, **2**, 9–43 (1982).

[7]J. Luo, H. Wang, and Y.-M. Chiang, "Origin of Solid State Activated Sintering in Bi_2O_3-Doped ZnO," *J. Am. Ceram. Soc.*, **82**, 916 (1999).

[8]E. Jud, Z. Zhang, W. Sigle, and L. J. Gauckler, "Microstructure of Cobalt Oxide Doped Sintered Ceria Solid Solutions," *J. Electroceram.*, **16**, 191–7 (2006).

[9]Z. L. Zhang, S. A. Wilfried, M. Ruhle, E. Jud, and L. J. Gauckler, "Microstructure Characterization of a Cobalt-Oxide-Doped Cerium-Gadolinium-Oxide by Analytical and High-Resolution Tem," *Acta Mater.*, **55** [8] 2907–17 (2007).

[10]J. G. Dash, A. M. Rempel, and J. S. Wettlaufer, "The Physics of Premelted Ice and its Geophysical Consequences," *Rev. Mod. Phys.*, **78**, 695–741 (2006).

[11]Q. S. Mei and K. Lu, "Melting and Superheating of Crystalline Solids: From Bulk to Nanocrystals," *Prog. Mater. Sci.*, **52** [8] 1175–262 (2007).

[12]J. Luo, "Stabilization of Nanoscale Quasi-Liquid Interfacial Films in Inorganic Materials: A Review and Critical Assessment," *Crit. Rev. Solid State Mater. Sci.*, **32** [1–2] 67–109 (2007).

[13]J. Luo and Y.-M. Chiang, "Wetting and Prewetting on Ceramic Surfaces," *Annu. Rev. Mater. Res.*, **38**, 227–49 (2008).

[14]J. Luo, V. K. Gupta, D. H. Yoon, and H. M. Meyer, "Segregation-Induced Grain Boundary Premelting in Nickel-Doped Tungsten," *Appl. Phys. Lett.*, **87**, 231902 (2005).

[15]J. G. Dash, "Surface Melting," *Contemp. Phys.*, **30** [2] 89–100 (1989).

[16]J. G. Dash, H. Fu, and J. S. Wettlaufer, "The Premelting of Ice and its Environmental Consequences," *Rep. Prog. Phys.*, **58**, 115–67 (1995).

[17]S. W. Chan, J. S. Liu, and R. W. Balluffi, "Test for a Possible Melting Transition in Grain-Boundaries in Aluminum Near the Melting-Point," *Scripta Metallurgica*, **19** [10] 1251–5 (1985).

[18]T. E. Hsieh and R. W. Balluffi, "Experimental Study of Grain Boundary Melting in Aluminum," *Acta Metall.*, **37**, 1637–44 (1989).

[19]A. M. Alsayed, M. F. Islam, J. Zhang, P. J. Collings, and A. G. Yodh, "Premelting at Defects within Bulk Colloidal Crystals," *Science*, **309**, 1207–10 (2005).

[20]M. Tang, W. C. Carter, and R. M. Cannon, "Diffuse Interface Model for Structural Transitions of Grain Boundaries," *Phys. Rev. B*, **73** [2] 024102 (2006).

[21]M. Tang, W. C. Carter, and R. M. Cannon, "Grain Boundary Order-Disorder Transitions," *J. Mater. Sci.*, **41**, 7691–5 (2006).

[22]J. Mellenthin, A. Karma, and M. Plapp, "Phase-Field Crystal Study of Grain-Boundary Premelting," *Phys. Rev. B*, **78** [18] 184110 (2008).

[23]J. J. Hoyt, D. Olmsted, S. Jindal, M. Asta, and A. Karma, "Method for Computing Short-Range Forces Between Solid-Liquid Interfaces Driving Grain Boundary Premelting," *Phys. Rev. E*, **79** [2] 020601 (2009).

[24]S. R. Phillpot, J. Wang, D. Wolf, and H. Gleiter, "Computer Simulation of the Structure and Dynamical Properties of Grain Boundaries in a Nano-crystalline Model Material," *J. Eng. Appl. Sci.*, **A204** [1–2] 76–82 (1995).

[25]D. Wolf, "High-Temperature Structure and Properties of Grain Boundaries: Long-Range vs. Short-Range Structural Effects," *Curr. Opin. Solid State Mater. Sci.*, **5**, 435–43 (2001).

[26]S. von Alfthan, P. D. Haynes, K. Kaski, and A. P. Sutton, "Are the Structures of Twist Grain Boundaries in Silicon Ordered at 0 K," *Phys. Rev. Lett.*, **96** [5] 055505 (2006).

[27]P. Keblinski, S. R. Phillpot, D. Wolf, and H. Gleiter, "On the Thermodynamic Stability of Amorphous Intergranular Films in Covalent Materials," *J. Am. Ceram. Soc.*, **80**, 717–32 (1997).

[28]P. Keblinski, S. R. Phillpot, and D. Wolf, "Thermodynamic Criterion for the Stability of Amorphous Intergranular Films in Covalent Materials," *Phys. Rev. Lett.*, **77** [14] 2965–8 (1996).

[29]A. Suzuki and Y. Mishin, "Atomic Mechanisms of Grain Boundary Diffusion: Low Versus High Temperatures," *J. Mater. Sci.*, **40**, 3155–61 (2005).

[30]M. Tang, W. C. Carter, and R. M. Cannon, "Grain Boundary Transitions in Binary Alloys," *Phys. Rev. Lett.*, **97** [7] 075502 (2006).

[31]J. W. Cahn, "Critical Point Wetting," *J. Chem. Phys.*, **66** [8] 3667–72 (1977).

[32]S. J. Dillon, M. Tang, W. C. Carter, and M. P. Harmer, "Complexion: A New Concept for Kinetic Engineering in Materials Science," *Acta Mater.*, **55** [18] 6208–18 (2007).

[33]B. B. Straumal and B. Baretzky, "Grain Boundary Phase Transitions and Their Influence on Properties of Ploycrystals," *Interf. Sci.*, **12**, 147–55 (2004).

[34]Y. Mishin, W. J. Boettinger, J. A. Warren, and G. B. McFadden, "Thermodynamics of Grain Boundary Premelting in Alloys. I. Phase-Field Modeling," *Acta Mater.*, **57** [13] 3771–85 (2009).

[35]J. Luo, "Grain Boundary Complexions: The Interplay of Premelting, Prewetting, and Multilayer Adsorption," *Appl. Phys. Lett.*, **95** [7] 071911 (2009).

[36]P. L. Williams and Y. Mishin, "Thermodynamics of Grain Boundary Premelting in Alloys. Ii. Atomistic Simulation," *Acta Mater.*, **57** [13] 3786–94 (2009).

[37]S. Divinski, M. Lohmann, C. Herzig, B. Straumal, B. Baretzky, and W. Gust, "Grain Boundary Melting Phase Transition in the Cu-Bi System," *Phys. Rev. B*, **71** 104104 (2005).

[38]M. P. Harmer, "Interfacial Kinetic Engineering: How Far Have We Come Since Kingery's Inaugural Sosman Address?," *J. Am. Ceram. Soc.*, **93** [2] 301–17 (2010).

[39]M. P. Harmer, "The Phase Behavior of Interfaces," *Science*, **332**, 182–3 (2011).

[40]S. J. Dillon and M. P. Harmer, "Multiple Grain Boundary Transitions in Ceramics: A Case Study of Alumnia," *Acta Mater.*, **55**, 5247–54 (2007).

[41]S. J. Dillon and M. P. Harmer, "Demystifying the Role of Sintering Additives with "Complexion"," *J. Eur. Ceram. Soc.*, **28** [7] 1485–93 (2008).

[42]S. J. Dillon and M. P. Harmer, "Relating Grain Boundary Complexion to Grain Boundary Kinetics Ii: Silica-Doped Alumina," *J. Am. Ceram. Soc.*, **91** [7] 2314–20 (2008).

[43]S. J. Dillon and M. P. Harmer, "Relating Grain-Boundary Complexion to Grain-Boundary Kinetics I: Calcia-Doped Alumina," *J. Am. Ceram. Soc.*, **91** [7] 2304–13 (2008).

[44]S. J. Dillon, M. P. Harmer, and G. S. Rohrer, "Influence of Interface Energies on Solute Partitioning Mechanisms in Doped Aluminas," *Acta Mater.*, **58** [15] 5097–108 (2010).

[45]S. J. Dillon, M. P. Harmer, and G. S. Rohrer, "The Relative Energies of Normally and Abnormally Growing Grain Boundaries in Alumina Displaying Different Complexions," *J. Am. Ceram. Soc.*, **93** [6] 1796–802 (2010).

[46]S. J. Dillon, M. P. Harmer, and J. Luo, "Grain Boundary Complexions in Ceramics and Metals: An Overview," *JOM*, **61** [12] 38–41 (2009).

[47]R. Pandit, M. Schick, and M. Wortis, "Systematics of Multilayer Adsorption Phenomena on Attractive Substrates," *Phys. Rev. B*, **26** [9] 5112–20 (1982).

[48]J. Luo and X. M. Shi, "Grain Boundary Disordering in Binary Alloys," *Appl. Phys. Lett.*, **92**, 101901 (2008).

[49]J. Luo, "Liquid-Like Interface Complexion: From Activated Sintering to Grain Boundary Diagrams," *Curr. Opin. Solid State Mater. Sci.*, **12** [5/6] 81–8 (2008).

[50]X. Shi and J. Luo, "Grain Boundary Wetting and Prewetting in Ni-Doped Mo," *Appl. Phys. Lett.*, **94** [25] 251908 (2009).

[51]X. Shi and J. Luo, "Decreasing the Grain Boundary Diffusivity in Binary Alloys with Increasing Temperature," *Phys. Rev. Lett.*, **105**, 236102 (2010).

[52]X. Shi and J. Luo, "Developing Grain Boundary Diagrams as a Materials Science Tool: A Case Study of Nickel-Doped Molybdenum," *Phys. Rev. B*, **84** [1] 014105 (2011).

[53]U. Tartagglino, T. Zykova-Timan, F. Ercolessi, and E. Tosatti, "Melting and Nonmelting of Solid Surface and Nanosystems," *Phys. Rep.*, **411**, 291–321 (2005).

[54]R. M. Cannon, M. Rühle, M. J. Hoffmann, R. H. French, H. Gu, A. P. Tomsia and E. Saiz, "Adsorption and Wetting Mechanisms at Ceramic Grain Boundaries," *Ceramic Trans. (Grain Boundary Engineering in Ceramics)*, **118**, 427–44 (2000).

[55]D. R. Clarke, "On the Equilibrium Thickness of Intergranular Glass Phases in Ceramic Materials," *J. Am. Ceram. Soc.*, **70** [1] 15–22 (1987).

[56]D. R. Clarke, T. M. Shaw, A. P. Philipse, and R. G. Horn, "Possible Electrical Double-Layer Contribution to the Equilibrium Thickness of Intergranular Glass Films in Polycrystalline Ceramics," *J. Am. Ceram. Soc.*, **76**, 1201–4 (1993).

[57]M. Bobeth, D. R. Clarke, and W. Pompe, "Diffuse Interface Description of Intergranular Films in Polycrystalline Ceramics," *J. Am. Ceram. Soc.*, **82**, 1537–46 (1999).

[58]R. M. Cannon and L. Esposito, "High Temperature Colloidal Behavior: Particles in Liquid Silicates," *Z. Metallkd.*, **90**, 1002–15 (1999).

[59]V. N. Semenov, B. B. Straumal, V. G. Glebovsky, and W. Gust, "Preparation of Fe-Si Single-Crystals and Bicrystals for Diffusion Experiments by the Electron-Beam Floating-Zone Technique," *J. Cryst. Growth*, **151** [1–2] 180–6 (1995).

[60]E. I. Rabkin, V. N. Semenov, L. S. Shvindlerman, and B. B. Straumal, "Penetration of Tin and Zinc Along Tilt Grain Boundaries 43° [100] in Fe-5 At.% Si Alloy: Premelting Phase Transition?," *Acta Metall. Mater.*, **39**, 627–39 (1991).

[61]B. B. Straumal, O. I. Noskovich, V. N. Semenov, L. S. Shvindlerman, W. Gust, and B. Predel, "Premelting Transition on 38<100> Tilt Grain Boundaries in (Fe- 10 At.% Si)-Zn Alloys," *Acta Metall. Mater.*, **40**, 795–801 (1992).

[62]B. B. Straumal, E. Rabkin, L. Shvindlerman, and W. Gust, "Grain Boundary Zinc Penetration in Fe-Si Alloys: Premelting Phase Transition on the Grain Boundaries," *Mater. Sci. Forum*, **126–128**, 391–4 (1993).

[63]B. B. Straumal, E. Rabkin, W. Lojkowski, W. Gust, and L. S. Shvindlerman, "Pressure Influence on the Grain Boundary Wetting Phase Transition in Fe-Si Alloys," *Acta Mater.*, **45** [5] 1931–40 (1997).

[64]J.-R. Lee, Y.-M. Chiang, and G. Ceder, "Pressure-Thermodynamic Study of Grain Boundaries: Bi Segregation in Zno," *Acta Mater.*, **45** [3] 1247–57 (1997).

[65]Y.-M. Chiang, H. Wang, and J.-R. Lee, "HREM and STEM of Intergranular Films at Zinc Oxide Varistor Grain Boundaries," *J. Microscopy*, **191** [3] 275–85 (1998).

[66]L. S. Chang, E. Rabkin, B. B. Straumal, B. Baretzky, and W. Gust, "Thermodynamic Aspects of the Grain Boundary Segregation in Cu(Bi) Alloys," *Acta Mater.*, **47**, 4041–6 (1999).

[67]L.-S. Chang, E. I. Rabkin, B. Straumal, P. Lejcek, S. Hofmann, and W. Gust, "Temperature Dependence of the Grain Boundary Segregation of Bi in Cu Polycrystals," *Scripta Metall. Mater.*, **37**, 729–35 (1997).

[68]B. B. Straumal, P. Zieba, and W. Gust, "Grain Boundary Phase Transitions and Phase Diagrams," *Int. J. Inorg. Mater.*, **3** [8] 1113–5 (2001).

[69]S. Divinski, M. Lohmann, and C. Herzig, "Grain Boundary Diffusion and Segregation of Bi in Cu: Radiotracer Measurements in B and C Regimes," *Acta Mater.*, **52**, 3973–82 (2004).

[70]O. Gutfleisch, M. A. Willard, E. Brück, C. H. Chen, S. G. Sankar, and J. P. Liu, "Magnetic Materials and Devices for the 21st Century: Stronger, Lighter, and More Energy Efficient," *Adv. Mater.*, **23** [7] 821–42 (2011).

[71]H. D. Ackler and Y.-M. Chiang, "Model Experiment on Thermodynamic Stability of Retained Intergranular Amorphous Films," *J. Am. Ceram. Soc.*, **80** [7] 1893–6 (1997).

[72]A. Avishai, C. Scheu, and W. D. Kaplan, "Intergranular Films at Metal-Ceramic Interfaces Part I – Interface Structure and Chemistry," *Acta Mater.*, **53** [5] 1559–69 (2005).

[73]C. Scheu, G. Dehm, and W. D. Kaplan, "Equilibrium Amorphous Silicon-Calcium-Oxygen Films at Interfaces in Copper-Alumina Composite Prepared by Melt Infiltration," *J. Am. Ceram. Soc.*, **84**, 623–30 (2000).

[74]M. Baram and W. D. Kaplan, "Intergranular Films at Au-Sapphire Interfaces," *J. Mater. Sci.*, **41** [23] 7775–84 (2006).

[75]A. Avishai and W. D. Kaplan, "Intergranular Films at Metal-Ceramic Interfaces Part II – Calculation of Hamaker Coefficient," *Acta Mater.*, **53**, 1571–81 (2005).

[76]M. Baram, D. Chatain, and W. D. Kaplan, "Nanometer-Thick Equilibrium Films: The Interface Between Thermodynmaics and Atomistics," *Science*, **332**, 206–9 (2011).

[77]K.-W. Kwon, H.-J. Lee, and R. Sinclair, "Solid-State Amorphization at Tetragonal-Ta/Cu Interfaces," *Appl. Phys. Lett.*, **75** [7] 935–7 (1999).

[78]J. Luo and Y.-M. Chiang, "Equilibrium-Thickness Amorphous Films on {11-20} Surfaces of Bi_2O_3-Doped Zno," *J. Eur. Ceram. Soc.*, **19**, 697–701 (1999).

[79]J. Luo and Y.-M. Chiang, "Existence and Stability of Nanometer-Thick Disordered Films on Oxide Surfaces," *Acta Mater.*, **48** [18–19] 4501–15 (2000).

[80]J. Luo, Y.-M. Chiang, and R. M. Cannon, "Nanometer-Thick Surficial Films in Oxides as a Case of Prewetting," *Langmuir*, **21**, 7358–65 (2005).

[81]H. Qian and J. Luo, "Nanoscale Surficial Films and a Surface Transition in V_2O_5-TiO_2-Based Ternary Oxide Systems," *Acta Mater.*, **56**, 4702–14 (2008).

[82]H. J. Qian and J. Luo, "Vanadia-Based Equilibrium-Thickness Amorphous Films on Anatase (101) Surfaces," *Appl. Phys. Lett.*, **91** [6] 061909 (2007).

[83]H. J. Qian, J. Luo, and Y. M. Chiang, "Anisotropic Wetting of Zno by Bi$_2$O$_3$ with and without Nanometer-Thick Surficial Amorphous Films," *Acta Mater.*, **56** [4] 862–73 (2008).

[84]A. Kayyar, H. J. Qian, and J. Luo, "Surface Adsorption and Disordering in LiFePO$_4$ Based Battery Cathodes," *Appl. Phys. Lett.*, **95** [22] 221905 (2009).

[85]H. Wang and Y.-M. Chiang, "Thermodynamic Stability of Intergranular Amorphous Films in Bismuth-Doped Zinc Oxide," *J. Am. Ceram. Soc.*, **81** [1] 89–96 (1998).

[86]I. MacLaren, R. M. Cannon, M. A. Gülgün, R. Voytovych, N. P. Pogrion, and C. Scheu et al., "Abnormal Grain Growth in Alumina: Synergistic Effects of Yttria and Silica," *J. Am. Ceram. Soc.*, **86**, 650 (2003).

[87]J. Luo, M. Tang, R. M. Cannon, W. C. Carter, and Y.-M. Chiang, "Pressure-Balance and Diffuse-Interface Models for Surficial Amorphous Films," *Mater. Sci. Eng. A*, **422**, 19–28 (2006).

[88]. H. French, "Origin and Applications of London Dispersion Forces and Hamaker Constants in Ceramics," *J. Am. Ceram. Soc.*, **83**, 2117–46 (2000).

[89]E. Bertrand, H. Dobbs, D. Broseta, J. Indekeu, D. Bonn, and J. Meunier, "First-Order and Critical Wetting of Alkanes on Water," *Phys. Rev. Lett.*, **85** [6] 1282–5 (2000).

[90]F. Brochard-Wyart, J.-M. di Meglio, D. Quéré, and P. G. de Gennes, "Spreading of Nonvolatile Liquids in a Continuum Picture," *Langmuir*, **7**, 335–8 (1991).

[91]J. N. Israelachvili, *Intermolecular and Surface Forces*, 4th edition. Academic Press Limited, London, 1994.

[92]R. M. German, "Diffusional Activated Sintering – Densification, Microstructure and Mechanical Properties," *Prog. Powder Met.*, **39**, 243–54 (1984).

[93]R. M. German, "The Identification of Enhanced Sintering Systems Through Phase Diagrams," *Mod. Dev. Powder Met.*, **15**, 253–73 (1985).

[94]J. H. Brophy, L. A. Shepard, and J. Wulff, "The Nickel-Activated Sintering of Tungsten"; pp. 113–35 in *Powder Metallurgy*, Edited by W. Leszynski. Interscience, New York, 1961.

[95]K. S. Hwang and H. S. Huang, "Identification of the Segregation Layer and its Effects on the Activated Sintering and Ductility of Ni-Doped Molybdenum," *Acta Mater.*, **51**, 3915–26 (2003).

[96]R. M. German and Z. A. Munir, "Hetero-Diffusion Model for Activated Sintering of Molybdenum," *J. Less-Common Metals*, **58** [1] 61–74 (1978).

[97]N. Eustathopoulos, M. Nicholas, and B. Drevet, *Wettabilty at High Temperatures*. Pergamon, Amsterdam, 1999.

[98]R. Benedictus, A. Böttger, and E. J. Mittemeijer, "Thermodynamic Model for Solid-State Amorphization in Binary Systems at Interfaces and Grain Boundaries," *Phys. Rev. B*, **54** [13] 9109–21 (1996).

[99]L. P. H. Jeurgens, Z. M. Wang, and E. J. Mittemeijer, "Thermodynamics of Reactions and Phase Transformations at Interfaces and Surfaces," *Int. J. Mater. Res.*, **100** (10), 1281–307 (2009).

[100]B. X. Liu, W. S. Lai, and Z. J. Zhang, "Solid-State Crystal-to-Amorphous Transition in Metal-Metal Multilayers and its Thermodynamic and Atomistic Modelling," *Adv. Phys.*, **50** (4), 367–420 (2001).

[101]J. S. Lee, K. Klockgeter, and C. Herzig, "Grain Boundary Self and Impurity Diffusion in Tungsten in the Tempearture Range of Activated Sintering," *Coll. Physique*, **51**, C1–569 (1990).

[102]L. P. H. Jeurgens, W. G. Sloof, F. D. Tichelaar, and E. J. Mittemeijer, "Thermodynamic Stability of Amorphous Oxide Films on Metals: Application to Aluminum Oxide Films on Aluminum Substrates," *Phys. Rev. B*, **62** [7] 4707–19 (2000).

[103]H. D. Ackler and Y.-M. Chiang, "Effect of Initial Microstructure on Final Intergranular Phase Distribution in Liquid Phase Sintered Ceramics," *J. Am. Ceram. Soc.*, **82** [1] 183–9 (1999).

[104]R. H. French, V. A. Parsegian, R. Podgornik, R. F. Rajter, A. Jagota, J. Luo, D. Asthagiri, M. K. Chaudhury, Y.-M. Chiang, S. Granick, S. Kalinin, M. Kardar, R. Kjellander, D. C. Langreth, J. Lewis, S. Lustig, D. Wesolowski, J. Wettlaufer, W.-Y. Ching, M. Finnis, F. Houlihan, O. A. von Lilienfeld, C. J. van Oss, and T. Zemb, "Long Range Interactions in Nanoscale Science," *Rev. Mod. Phys.*, **82** [2] 1887–944 (2010).

[105]U. R. Kattner, "The Thermodynamic Modeling of Multicomponent Phase Equilibria," *JOM*, **49** [12] 14–9 (1997).

[106]L. S. Chang and K. B. Huang, "Temperature Dependence of the Grain Boundary Segregation of Bi in Ni Polycrystals," *Scripta Mater.*, **51** [6] 551–5 (2004).

[107]S. Ma, K. Meshinchi Asl, C. Tansarawiput, P. R. Cantwella, M. Qi, and M. P. Harmer et al., "A Grain-Boundary Phase Transition in Si-Au," *Scripta Mater.*, **66**, 203–6 (2012).

[108]R. Kobayashi, J. A. Warren, and W. C. Carter, "A Continuum Model of Grain Boundaries," *Phys. D*, **140**, 141–51 (2000).

[109]J. Luo, H. Cheng, K. M. Asl, C. J. Kiely, and M. P. Harmer, "The Role of a Bilayer Interfacial Phase on Liquid Metal Embrittlement," *Science*, **333** [6050] 1730–3 (2011).

[110]E. H. Conrad, "Surface Roughening, Melting, and Faceting," *Prog. Surf. Sci.*, **39** [1] 65–116 (1992).

[111]J. W. Cahn, "Transition and Phase Equilibria Among Grain Boundary Structures," *J. Phys.-Paris*, **43**, C6 (1982).

[112]I. Daruka and J. C. Hamilton, "Atomistic and Lattice Model of a Grain Boundary Defaceting Phase Transition," *Phys. Rev. Lett.*, **92**, 246105 (2004).

[113]S. M. An and S. J. L. Kang, "Boundary Structural Transition and Grain Growth Behavior in BaTiO$_3$ with Nd$_2$O$_3$ Doping and Oxygen Partial Pressure Change," *Acta Mater.*, **59** [5] 1964–73 (2011).

[114]Y. H. Heo, S. C. Jeon, J. G. Fisher, S. Y. Choi, K. H. Hur, and S. J. L. Kang, "Effect of Step Free Energy on Delayed Abnormal Grain Growth in a Liquid Phase-Sintered BaTiO$_3$ Model System," *J. Eur. Ceram. Soc.*, **31** [5] 755 –62 (2011).

[115]S. J. L. Kang, M. G. Lee, and S. M. An, "Microstructural Evolution During Sintering with Control of the Interface Structure," *J. Am. Ceram. Soc.*, **92** [7] 1464–71 (2009).

[116]M. G. Lee, S. Y. Chung, and S. J. L. Kang, "Boundary Faceting-Dependent Densification in a BaTiO$_3$ Model System," *Acta Mater.*, **59** [2] 692–8 (2011).

[117]B. K. Yoon, S. Y. Choi, T. Yamamoto, Y. Ikuhara, and S. J. L. Kang, "Grain Boundary Mobility and Grain Growth Behavior in Polycrystals with Faceted Wet and Dry Boundaries," *Acta Mater.*, **57** [7] 2128–35 (2009).

[118]Y. K. Cho, S. J. L. Kang, and D. Y. Yoon, "Dependence of Grain Growth and Grain-Boundary Structure on the Ba/Ti Ratio in BaTiO$_3$," *J. Am. Ceram. Soc.*, **87** [1] 119–24 (2004).

[119]S. Y. Choi and S. J. L. Kang, "Sintering Kinetics by Structural Transition at Grain Boundaries in Barium Titanate," *Acta Mater.*, **52** [10] 2937–43 (2004).

[120]S. Y. Chung, S. J. L. Kang, and V. P. Dravid, "Effect of Sintering Atmosphere on Grain Boundary Segregation and Grain Growth in Niobium-Doped SrTiO$_3$," *J. Am. Ceram. Soc.*, **85** [11] 2805–10 (2002).

[121]S. Y. Chung, D. Y. Yoon, and S. J. L. Kang, "Effects of Donor Concentration and Oxygen Partial Pressure on Interface Morphology and Grain Growth Behavior in SrTiO$_3$," *Acta Mater.*, **50** [13] 3361–71 (2002).

[122]Y. I. Jung, S. Y. Choi, and S. J. L. Kang, "Effect of Oxygen Partial Pressure on Grain Boundary Structure and Grain Growth Behavior in BaTiO$_3$," *Acta Mater.*, **54** [10] 2849–55 (2006).

[123]B. K. Lee, S. Y. Chung, and S. J. L. Kang, "Grain Boundary Faceting and Abnormal Grain Growth in BaTiO$_3$," *Acta Mater.*, **48** [7] 1575–80 (2000).

[124]G. Gottstein and D. A. Molodov, "Grain Boundary Migration in Metals: Recent Developments," *Interf. Sci.*, **6**, 7–22 (1998).

[125]D. Weygand, Y. Breichet, E. Rabkin, B. Straumal, and W. Gust, "Solute Drag and Wetting of a Grain Boundary," *Philos. Mag. Lett.*, **76** [3] 133–8 (1997).

[126]X. Feng, D. S. Sayle, Z. L. Wang, M. S. Paras, B. Santora, A. C. Sutorik et al., "Converting Ceria Polyhedral Nanoparticles into Single-Crystal Nanospheres," *Science*, **312**, 1504–8 (2004).

[127]P. F. Becher, G. S. Painter, E. Y. Sun, C. H. Hsueh, and M. J. Lance, "The Importance of Amorphous Intergranular Films in Self-Reinforced Si$_3$N$_4$ Ceramics," *Acta Mater.* [48] 4493–9 (2000).

[128]P. F. Becher, G. S. Painter, M. J. Lance, S. Li, and Y. Ikuhara, "Direct Observations of Debonding of Reinforcing Grains in Silicon Nitride Ceramics Sintered with Yttria Plus Alumina Additives," *J. Am. Ceram. Soc.*, **88** [5] 1222 –6 (2005).

[129]P. F. Becher, E. Y. Sun, C. H. Hsueh, G. S. Painter, and K. L. More, "Role of Intergranular Films in Toughened Ceramics," *Key Eng. Mater.*, **175– 176**, 97–106 (2000).

[130]X.-F. Zhang, M. E. Sixta, and L. C. DeJonghe, "Grain Boundary Evolution in Hot-Pressed ABC-SiC," *J. Am. Ceram. Soc.*, **83** [11] 2813–20 (2000).

[131]R. Brydson, P. C. Twigg, F. Loughran, and F. L. Riley, "Influence of CaO-SiO$_2$ Ratio on the Chemistry of Intergranular Films in Liquid-Phase Sintered Alumina and Implications for Rate of Erosive Wear," *J. Mater. Res.*, **16** [3] 652–65 (2001).

[132]P. Svancarek, D. Galusek, C. Calvert, F. Loughran, A. Brown, R. Brydson et al., "A Comparison of the Microstructure and Mechanical Properties of Two Liquid Phase Sintered Aluminas Containing Different Molar Ratios of Calcia-Silica Sintering Additives," *J. Eur. Ceram. Soc.*, **24** [12] 3453–63 (2004).

[133]S. Primdahl, A. Tholen, and T. G. Langdon, "Microstructural Examination of a Superplastic Yttria-Stabilized Zirconia: Implications for the Superplasticity Mechanism," *Acta Metall. Mater.*, **43**, 1211–8 (1995).

[134]V. Jayaram and R. Sinclair, "Detection of Thin Intergranular Cobalt Layers in WC-Co Composites by Lattice Imaging," *J. Am. Ceram. Soc.*, **66**, C137–9 (1983).

[135]Y.-M. Chiang, L. A. Silverman, R. H. French, and R. M. Cannon, "Thin Glass Film Between Ultrafine Conductor Particles in Thick-Film Resistors," *J. Am. Ceram. Soc.*, **77**, 143–52 (1994).

[136]H. Nakano, K. Watari, and K. Urabe, "Grain Boundary Phase in AlN Ceramics Fired Under Reducing N$_2$ Atmosphere with Carbon," *J. Eur. Ceram. Soc.*, **23**, 1761–8 (2003).

[137]D. L. Callahan and G. Thomas, "Impurity Distribution in Polycrystalline Aluminum Nitride Ceramics," *J. Am. Ceram. Soc.*, **73**, 2167–70 (1990).

[138]R. Ramesh, S. M. Green, and G. Thomas, "Microstructure Property Relations in the Bi(Pb)-Sr-Ca-Cu-O Ceramic Superconductors," pp. 363–403, in *Studies of High Temperature Superconductors: Advances in Research and Applications*, Vol. 5, Edited by A. Narlikar. Nova Science Publ., Commack, NY, 1990.

[139]G. J. Zhang, R. Yu, S. Vyas, J. Stettler, J. A. Reimer, and G. Harley et al., "Proton Conduction and Characterization of an La(PO3)$_3$-Ca(PO3)$_2$ Glass-Ceramic," *Solid State Ionics*, **178** [35–36] 1811–6 (2008).

[140]B. Kang and G. Ceder, "Battery Materials for Ultrafast Charging and Discharging," *Nature*, **458** [7235] 190–3 (2009).

[141]M. Tang, H. Y. Huang, N. Meethong, Y. H. Kao, W. C. Carter, and Y. M. Chiang, "Model for the Particle Size, Overpotential, and Strain Dependence of Phase Transition Pathways in Storage Electrodes: Application to Nanoscale Olivines," *Chem. Mater.*, **21** [8] 1557–71 (2009).

[142]K. Sun and S. J. Dillon, "A Mechanism for the Improved Rate Capability of Cathodes by Lithium Phosphate Surficial Films," *Electrochem. Commun.*, **13** [2] 200–2 (2011).

[143]X. B. Chen, L. Liu, P. Y. Yu, and S. S. Mao, "Increasing Solar Absorption for Photocatalysis with Black Hydrogenated Titanium Dioxide Nanocrystals," *Science*, **331** [6018] 746–50 (2011). □
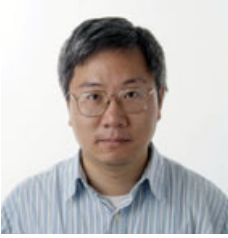
Jian Luo graduated from Tsinghua University with dual Bachelor's degrees, one in Materials Science and Engineering and another in Electronics and Computer Technology. He received a M.S. degree in Materials Science and Engineering in 1999, and a Ph.D. degree in Ceramics in 2001, both from M.I.T.. After working in the industry with Lucent Technologies and OFS for more than two years, he joined the Clemson faculty as an Assistant Professor in the School of Materials Science and Engineering and the Center for Optical Materials Science and Engineering Technology in 2003. He was promoted to an Associate Professor in 2009 and a Professor in 2012 (effective August 15). Luo's research group is conducting fundamental studies on solid interfaces and their roles in controlling materials fabrication and properties. Current projects are focused on utilizing nanoscale interfacial phenomena to design and tailor materials for energy-related applications. Luo received a National Science Foundation CAREER award in 2005 and an Air Force Office of Scientific Research Young Investigator award in 2007. He currently serves as the Vice Chair for the Basic Science Division of the American Ceramic Society.